DEER Experiments Reveal Fundamental Differences between Calmodulin Complexes with IQ and MARCKS Peptides in Solution

Chandrima Jash,[1,#] Akiva Feintuch,[1,#] Shira Naor,[1] Nurit Manukovsky,[1] Elwy H. Abdelkader,[2] Sudeshna Bhattacharya,[1] Gunnar Jeschke,[3] Gottfried Otting,[2] Daniella Goldfarb*[1]

[1]Department of Chemical and Biological Physics, Weizmann Institute of Science, Rehovot Israel.

[2] ARC Centre of Excellence for Innovations in Peptide & Protein Science, Research School of Chemistry, Australian National University, Canberra, ACT 2605, Australia.

[3] Laboratory of Physical Chemistry, ETH Zürich, Switzerland.

[#] These authors contributed equally.

Summary

Calmodulin (CaM) is a calcium binding protein regulating the function of many other proteins by indirectly conferring Ca^{2+} sensitivity. It comprises two globular domains, each of which binds two Ca^{2+} ions, connected by a flexible linker. Extensive structural studies revealed that CaM binds to helical polypeptide segments of binding partners, with its N- and C-domains wrapping around the peptide leading to a closed conformation. This work compares the binding mode of two such peptides, MARCKS and IQ, for which crystal structures revealed closed conformation. To assess the structures in solution, we performed double electron-electron resonance (DEER) experiments employing labelling schemes involving nitroxide and Gd(III) spin labels as well as specific substitution of one of the Ca^{2+} ions in the CaM mutant N60D by a Gd(III) ion. We measured Gd(III)–Gd(III), Gd(III)–nitroxide and nitroxide–nitroxide distances distributions to track conformational changes and peptide binding. We found that MARCKS binds to CaM in both the *apo*- and *holo*-states, but binding to *holo*-CaM resulted neither in a closed conformation nor in a unique relative orientation between the two domains. This was supported by NMR measurements of pseudocontact shifts of the N60D mutant with paramagnetic lanthanoid ions. In contrast, binding of IQ to *holo*-CaM generated a closed conformation. Using the elastic network model and 12 distance restraints obtained from multiple *holo*-CaM/IQ DEER data, we derived a model of the solution structure, which is in reasonable agreement with the crystal structure. The data reveal structural disorder of the IQ peptide at both termini and some disorder in the EF loop with Gd(III).

Keywords

Calmodulin, Protein-peptide interaction, EPR, DEER, NMR, IQ-peptide, MARCKS, Lanthanoid ions.

Introduction

Proteins exhibiting high flexibility are often associated with a wide range of biological functions enabled by interactions with many other proteins, often referred to as clients. Calmodulin (calcium modulated protein, CaM) is a classic example of such a protein.(Ikura et al., 1992) In this case, the structural flexibility resides predominantly in the unstructured linker connecting its N- and C-domains. Flexible proteins are most effectively studied by spectroscopic techniques, including double electron-electron resonance (DEER or PELDOR).(Jeschke, 2012b) This technique measures nanometre scale distance distributions between spin labels attached at well-defined positions in the proteins and the measurements are usually carried out in frozen solutions. In a distance distribution, the mean distance provides the most easily interpretable piece of structural information, whereas the width of the distance distribution contains qualitative important information on the degree of conformational heterogeneity captured during the freezing of the sample. Notably, the flexibility of the spin label contributes to the width of the distance distribution and therefore spin labels with minimal flexibility are preferred if backbone structure is expected to be well defined and as long as the labels are not expected to bias the structure.(Marko et al., 2011) In this work, we performed DEER experiments with non-standard labelling schemes, some of which weredesigned to minimize the label contribution to the distance distribution, and tracked the conformational changes of CaM in response to the binding of two different target peptides. We complemented these measurements with by paramagnetic NMR measurements. A major difference between solution NMR and EPR spectroscopy is the state of the sample; NMR measurements are carried out at room temperature and conformational heterogeneity is often averaged. In contrast, the DEER experiment is carried out on frozen solutions, where conformational heterogeneity is preserved and trapped during freezing, contributing to the width of the distance distribution.

Calmodulin is a small (about 17 kDa, 148 residues) intracellular Ca^{2+} sensing protein present in almost all eukaryotic organisms, which is known to regulate the function of many other proteins by conferring Ca^{2+} sensitivity.(Yamniuk and Vogel, 2004) Different proteins can bind CaM in many different ways (Yamniuk and Vogel, 2004; Yap et al., 2000) and the actual mechanism of activation is only incompletely understood for most of them. This is, in part, because many CaM targets are large multimeric or transmembrane proteins,(Hovey et al., 2017; Kumar et al., 2013b; Thomas

and Timson, 2018) which are hard to study by standard structure determination methods. Accordingly, most of the structural studies focused on target proteins that CaM binds to by capturing small polypeptide segments.(Vetter and Leclerc, 2003)

CaM comprises two structurally similar domains, the N- and C-domains, which are connected by a highly flexible linker peptide. The flexibility of this linker is believed to play a key role in enabling CaM to interact with many different targets.(Yamniuk and Vogel, 2004) The N- and C- domains each contain a pair of EF hands, which are carboxylate-rich loops framed by two helices.(Ogawa and Tanokura, 1984; Potter et al., 1983) CaM adopts different conformations in response to Ca^{2+} binding. The *apo* state in the absence of Ca^{2+} ions is characterized by a "closed" conformation of the N-domain and a "semi-open" conformation of the C-domain.(Houdusse and Cohen, 1995; Yamniuk and Vogel, 2004) In the *apo* state, the C-domain can bind some targets while the N-domain makes few contacts with target proteins or the C-domain of CaM.(Hovey *et al.*, 2017; Yamniuk and Vogel, 2004) In the *holo* form of fully Ca^{2+}-loaded CaM (Ca^{2+}/CaM), the protein conformation exposes hydrophobic amino acids of both domains, which facilitates interactions with target proteins, but it still retains high linker flexibility, allowing the N- and C-domains to sample many different relative orientations in solution.(Gigli et al., 2018) CaM conformational heterogeneity has been studied by NMR using residual dipolar couplings (RDC), pseudocontact shifts (PCS),(Russo et al., 2013; Ye et al., 2017) paramagnetic relaxation enhancements (PRE) (Anthis et al., 2011)as well as small-angle X-ray scattering (SAXS) (Kataoka et al., 1991) and DEER measurements.(Her et al., 2018)

There is no single mode of target binding and activation/deactivation by CaM. Most, but not all, high-resolution crystal structures of Ca^{2+}/CaM in complex with target peptides depict CaM enclosing the CaM-binding motif of the target peptide, assuming a conformation akin to the a closed conformation, sometimes referred to as collapsed conformation shown in Fig. 1.(Ikura *et al.*, 1992; Meador et al., 1992; Osawa et al., 1999; Schumacher et al., 2001) The bound target peptide usually assumes a mostly α-helical conformation and resides in a hydrophobic channel formed by the two lobes of Ca^{2+}/CaM. The target peptides are often characterized by at least two hydrophobic anchor residues at positions 1/10, 1/12, 1/14, 1/16,(Osawa *et al.*, 1999) 1/17(Maximciuc et al., 2006) and 1/10/14 for three anchors,(Gifford et al., 2007) which bind in two hydrophobic pockets formed by the N- and C-domains of CaM. Several peptides, such as the

IQ peptide, bind CaM in both the *apo*- and *holo*-states.(Chagot and Chazin, 2011; Fallon et al., 2005)

We focused on two peptides, with the MARCKS and IQ motifs, which have been reported to exhibit different binding modes. The MARCKS peptide is a CaM-binding motif from myristoylated alanine-rich C kinase substrate, which is a membrane-associated protein essential for the development of the central nervous system.(Matsubara et al., 1998) MARCKS binds tightly to Ca^{2+}/CaM with a dissociation constant, K_d, of 8.8 nM.(Yamauchi et al., 2003) The crystal structure of the Ca^{2+}/CaM/MARCKS complex shows a closed conformation (Porumb et al., 1997a) similar to those of classical peptide-CaM complexes. In the complex, the MARCKS peptide forms only a short helix, in contrast to classical complexes where the peptides are found to form a long α-helix. This observation was supported by circular dichroism (CD) and NMR studies (Matsubara *et al.*, 1998; Porumb *et al.*, 1997a) and stands in contrast to an early CW-EPR study, which argued for a longer helix based on reduced mobility observed for nitroxide spin labels situated along the MARCKS peptide sequence in the complex.(Qin et al., 1996) Unlike classical CaM-binding peptides, the anchor residues of the MARCKS peptide are separated by a single residue only and the crystal structure indicates that one is buried deep in a binding pocket, whereas the other interacts more superficially with the hydrophobic surface of the N-domain, while the hydrophobic pocket of the N-domain is almost absent.(Yamauchi *et al.*, 2003) To date, there are no reports on MARCKS binding to *apo*-CaM.

The second peptide studied in the present work is the IQ peptide which comprises the IQ-motif sequence IQXXXRGXXXR. The conserved residues in this motif are not the only determinants of binding,(Hovey *et al.*, 2017; Vetter and Leclerc, 2003) as different variants of IQ peptides differ in their binding affinity to CaM states.(Kumar et al., 2013a) The IQ peptide used in the present work was derived from the CaV1.2 calcium channel.(Fallon *et al.*, 2005) Its crystal structure in the presence of Ca^{2+} contains three CaM molecules in the asymmetric unit, which display different conformations with different orientations of the N-domain relative to the C-domain.(Fallon *et al.*, 2005) NMR measurements with the same IQ peptide indicated that the solution structure is best described by an ensemble of up to 8 conformers that are in fast exchange on the NMR time scale, with three of those conformations corresponding to those observed in the crystal structure and the others obtained from molecular dynamic simulations.(Russo *et al.*, 2013) DEER has previously been applied to probe the conformational changes of CaM upon binding of an IQ peptide and the

formation of a closed conformation was observed both *in vitro* and in cell extract using CaM doubly labelled with Gd(III) spin labels, while no conformational change was observed in cells.(Dalaloyan et al., 2019)

In this work, we explore the binding of MARCKS and IQ peptides to both *apo*- and *holo*-CaM in solution to explore the potential of DEER measurements to capture the conformational heterogeneity in solution and resolve the impact of different peptides, with the CaM/IQ complex serving as a reference. To this end we combined several labelling schemes: (i) CaM labelled with Gd(III) spin labels in the C- and N-domains to track the formation of closed conformations by Gd(III)–Gd(III) DEER.(Giannoulis et al., 2021) (ii) Use of the CaM-N60D mutant to introduce a Gd(III) ion in one of the EF loops of the N-terminal domain and thus eliminate the contribution of a flexible spin-label linker from the width of the distance distribution. The N60D mutant has been shown to have a very high affinity for lanthanide ions even in the presence of excess Ca^{2+} ions, permitting the preparation of well defined $(CaLn)_N(Ca_2)_C$CaM derivatives.(Bertini et al., 2003) In this case, the second spin label was a nitroxide (NO) placed in the C-domain with the aim to track the formation of the closed conformation. Paramagnetic NMR has previously used this labelling scheme successfully to probe CaM conformations.(Bertini et al., 2009; Russo *et al.*, 2013) As a control of structural integrity of the N-domain in the N60D mutant, a sample was also prepared with an NO label in the N-domain. These samples were subjected to Gd(III)–NO DEER.(Lueders et al., 2011) (iii) Samples with spin labels in CaM and the bound peptide to establish binding to the C- or N-domains. The peptide was labelled with NO and CaM was labelled with a Gd(III) spin label in either the N- or C-domains, or labelled with Gd(III) in the EF loop using the N60D mutant. NO–Gd(III) DEER was performed, which in this case is preferable to Gd(III)–Gd(III) or NO–NO DEER as it eliminates potential contributions from CaM dimers, which have been reported in solution.(Lafitte et al., 1999a) Fig. 1 illustrates the labelling positions in the crystal structures of *holo*-CaM/IQ and *holo*-Cam/MARCKS and the chemical structures of the spin labels are shown in Fig.2.

Finally, we recorded NMR data of *holo*-CaM N60D loaded with paramagnetic lanthanoid ions to measure pseudocontact shifts (PCS) and assess the structural integrity of the N-domain in solution and the mobility of the C-domain relative to the N-domain in the presence of MARCKS peptide. These data provide a picture of the CaM/MARCKS complex at 25 °C, which complements the DEER data obtained in frozen solution.

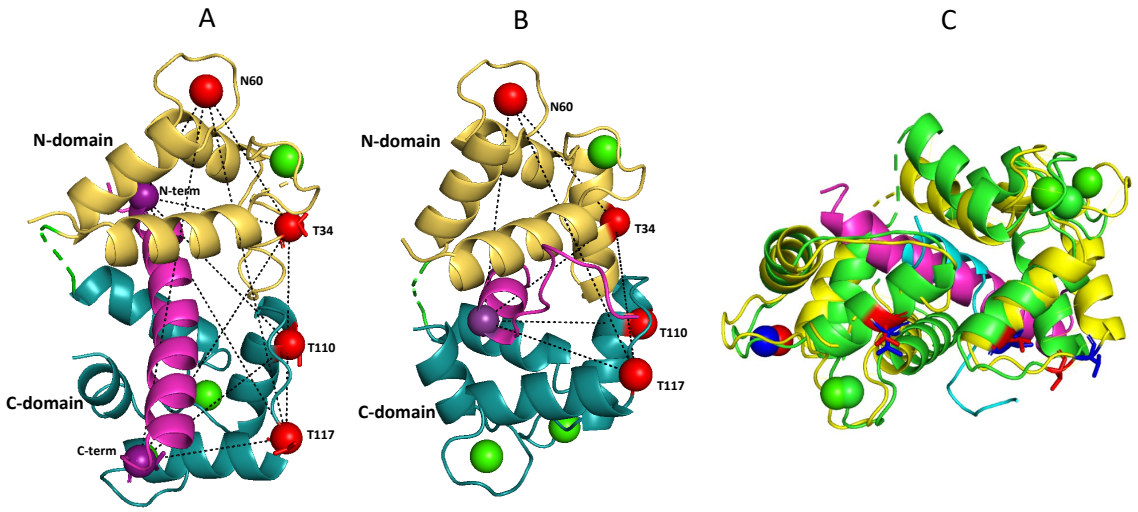

Fig. 1. Crystal structures of (A) *holo*-CaM/IQ (PDB 2BE6, chain A)(Fallon *et al.*, 2005) and (B) *holo*-CaM/MARCKS (PDB 1IWQ).(Yamauchi *et al.*, 2003) The C-domain is colored deep teal, the N-domain light orange and bound peptide pink. The Gd(III) ion replacing one of the Ca^{2+} ions in the N60D mutant is indicated in red and the Ca^{2+} ions are green. Red and purple balls identify CaM and peptide residues labelled with tags, respectively. Lines connecting the labelling sites indicate pairs subjected to DEER measurements (C) Superimposition of the structures shown in (A) and (B). The positions of some of the labelling sites are shown in red and blue for the complex with the MARCKS and IQ peptide, respectively. The IQ peptide is shown in magenta and the MARCKS peptide in cyan. The structure 2BE6 is colored yellow and 1IWQ green.

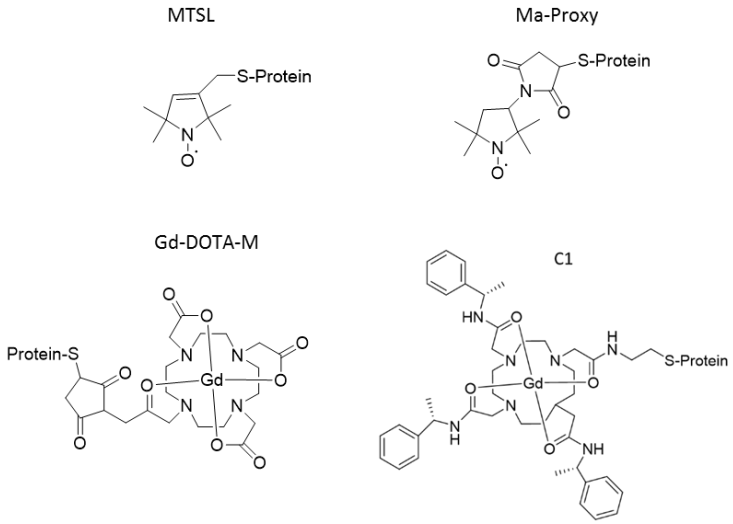

Figure 2. Spin labels used in this study.

Results

CaM conformational changes upon MARCKS and IQ binding

Initially we aimed at mapping the conformational changes Ca^{2+}/CaM undergoes upon binding of MARCKS. For this we prepared a series of nine double-cysteine mutants (Table S1) labelled with the Gd-C1 tag (Fig. 2C), where one label was located in the N-domain and the other in the C-domain. We designed this labelling scheme to detect the expected closure of the two domains in the presence of target peptides. The Gd(III)–Gd(III) DEER data in the presence and absence of MARCKS are presented in Figs S1-S3 and the results were unexpected. The experimental distance distributions deviated very much from those predicted from the crystal structure and they were very broad and only two of the 9 constructs, T34C/A103C and T34C/119C, showed a significant distance change upon addition of MARCKS. In contrast, we observed in an earlier study that Ca^{2+}/CaM T34C/117C labelled with Gd-DOTA-M displayed a shorter distance between N- and C-domain upon binding of the IQ peptide.(Dalaloyan *et al.*, 2019) Therefore, we prepared this mutant as well and labelled it with Gd-DOTA-M. Again, we found no evidence of a closed conformation following the addition of MARCKS, in stark contrast to IQ (Fig. 3A), where there is good agreement with the distances predicted for all three conformations observed in the crystal structure (see below).

To reduce the uncertainty in the distance distribution contributed by the size and flexibility of the tags, and to minimize the possibility that the tags interfered with the binding affinity to MARCKS, we prepared two new mutants N60D/T117C and N60D/T34C. Here Gd(III) substituted one of the Ca^{2+} ions in the N-domain as afforded by the N60D mutation.(Bertini *et al.*, 2003; Bertini *et al.*, 2009) Representative echo-detected EPR spectra of CaM labelled with Gd-DOTA-M and the Gd(III)-N60D mutant are depicted in Fig. S4. The Gd(III)-N60D mutant displayed a much larger zero-field-splitting (ZFS) compared to Gd-DOTA-M, as manifested by its broader central transition. This large ZFS would lead to a low modulation depth and therefore we labelled these mutants with a nitroxide (MA-proxyl) as the second label (Table 1). The X-band EPR spectrum of the nitroxide-labelled mutant N60D/T117C is shown in Fig. S5 and revealed high mobility independent of the presence of Ca^{2+} or peptide. The N60D/T117C mutant was designed to probe the inter-domain movement, whereas the N60D/T34C mutant was designed to probe any intra-domain movement within the N-domain, which is expected to be quite rigid.

Figs. 3B, C show W-band Gd–NO DEER data obtained from these samples in the presence and absence of MARCKS. For the data obtained with nitroxide tags, one has to consider the possibility of orientation selection,(Kaminker et al., 2013) in particular for narrow distance distributions. These effects were reduced by the choice of pump pulse frequency and the use of a linear chirp pump pulse (Fig. S4). The experimental distance distributions reveal notable differences to those predicted from the available crystal structure. We observe a broad distance distribution for the N60D/T117C mutant, which probes the inter-domain distance, without any indication of a conformational change induced by the MARCKS peptide, although we confirmed peptide binding (see below). In contrast, CaM N60D/T34C in the presence of MARCKS produced a short distance, which is close to the predicted distance, and a relatively narrow distance distribution. As expected for this intra-domain distance, it did not change much between the protein with and without the peptide.

In contrast, the DEER data of N60D-Gd(III)/T117C-MA-proxyl showed a difference upon IQ binding (Fig. 3B), manifested clearly in the time domain data, but the distance distribution was broad. In the presence of the IQ peptide, the distance distribution shows two maxima around 3 nm and 4.3 nm, which were reproduced in repeat experiments. The N60D-Gd(III)/T34C-MA-proxyl construct responded similarly to the binding of IQ peptide (Fig. 3C) as it did in response to the MARCKS peptide, showing a short distance that did not change significantly upon IQ binding. Both with MARCKS and IQ peptide, this intra-domain measurement showed a low modulation depth which may indicate the presence of short distances that cannot be accessed experimentally by DEER experiments.

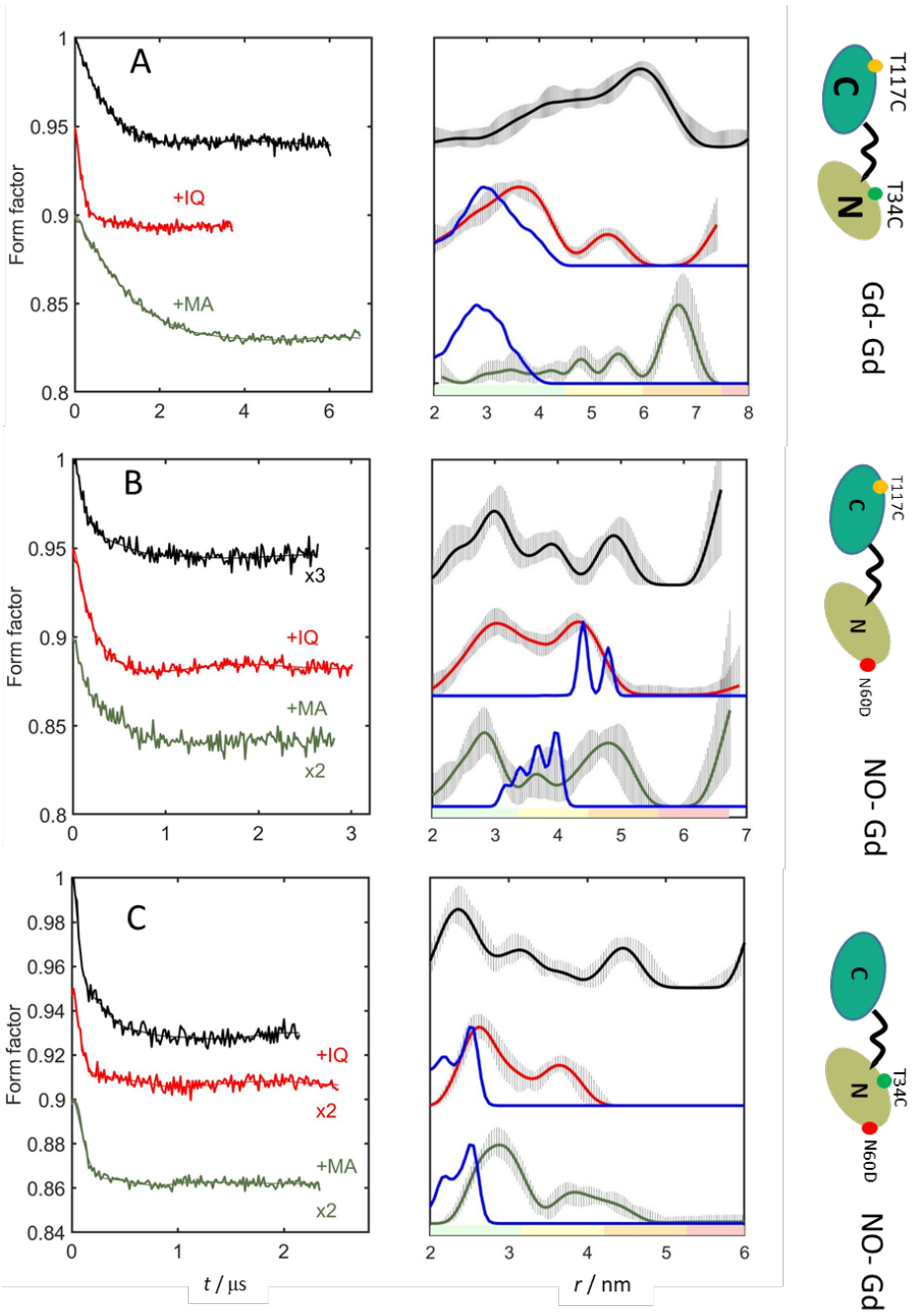

Figure 3. DEER data of Ca^{2+}-CaM labelled in different ways, free and with MARCKS or IQ peptides. (A) Gd(III)–Gd(III) DEER of the mutant T34C/T117C-Gd-DOTA-M. (B) Gd(III)–NO DEER of the mutant T34C-MA-proxyl/N60D-Gd(III). (C) Gd(III)–NO DEER of the mutant T117C-MA-proxyl/N60D-Gd(III). The panels on the left show the DEER data after the background removal along with the fitted trace. Traces that had low modulation depth were expanded by a factor as noted in the figure. The panels in the middle column show the corresponding distance distributions along with the distance distribution predicted from the respective crystal structures (blue, using chain A for the IQ data). The colour bar underneath the distance distributions shows the reliability regions as defined in DeerAnalysis, determined by the DEER evolution time (green: the shape of the distance distribution is reliable; yellow: the mean distance and distribution width

are reliable; orange: the mean distance is reliable; red: unreliable long-range distances). The solid lines represent the distributions with the smallest r.m.s.d. to the experimental data and the striped regions indicate the range of alternative distributions ($\pm$2 times the standard deviation) obtained by varying the parameters of the background correction and noise as calculated by the validation tool in the DeerAnalysis software package with the default values.(Jeschke et al., 2006) The primary DEER data are shown in Fig. S6. The right column presents cartoons of CaM with the labelling sites.

CaM is known to be prone to form non-covalent dimers,(Lafitte et al., 1999b) which can be suppressed by increased salt concentrations.(Bertini et al., 2012) To assess dimer formation in our samples, we carried out control Gd(III)–Gd(III) DEER measurements on the singly-labelled Gd-DOTA-M CaM mutants T117C and T34C as well as the N60D mutant. DEER modulations observed prior to the addition of salt indeed indicated the formation of dimers, whereas the addition of 200 mM KCl resulted in much shallower modulation depths in agreement with a negligible amount of oligomers (Fig. S7). Further reduction in the amount of dimers could be achieved by decreasing the CaM concentration. Therefore, the CaM concentration was kept at 50 μM and all samples listed in Table 1 contained 200 mM KCl. Furthermore, the application of Gd(III)–NO DEER reduces the contributions from dimers to the DEER traces as compared to Gd(III)–Gd(III) or NO–NO measurements, because inter-molecular same-tag contributions would hardly contribute to the Gd(III)–NO DEER.

To summarize, the binding of MARCKS to Ca^{2+}/CaM did not reveal the expected closure of the N- and C-domain as suggested by the crystal structure, instead indicating significant flexibility of the linker between N- and C-domain. Unlike MARCKS, the IQ peptide indicated closure of the N- and C-domains as observed earlier, although the complex with the IQ peptide also shows evidence of conformational heterogeneity. To investigate the Ca^{2+}/CaM/MARCKS complex in more detail, we proceeded to explore the protein–peptide interaction directly by DEER measurements between labelled MARCKS and labelled CaM, comparing the results with those obtained with the IQ peptide.

CaM interaction with MARCKS

To confirm the binding of MARCKS peptide and obtain information regarding its binding location in CaM, we carried out Gd(III)–NO DEER on the MARCKS mutant K164C labelled with MTSL and singly Gd(III)-labelled CaM. Specifically, the mutants T34C, T110C and T117C were labelled with Gd-DOTA-M and we also used the N60D-Gd(III) construct (Table 1). We probed both the binding

to *apo*-CaM (treated with 3 mM EDTA) and *holo*-CaM (in the presence of 5 mM $CaCl_2$). The N60D-Gd(III) variant was not measured in the *apo* state because the addition of EDTA removed also Gd(III). X-band CW EPR measurements of MARCKS K164C-MTSL in the presence of various amounts of Ca^{2+}/CaM T117C (Fig. S8) showed the appearance of a spectral component indicative of a nitroxide with restricted motion, the relative intensity of which increased with increasing CaM concentration. The restricted motion is consistent with an earlier EPR report (Qin *et al.*, 1996) and clearly indicates binding of the peptide. In the case of *apo*-CaM, only minor broadening was detected with increasing CaM concentration.

The DEER results presented in Fig. 4 demonstrate that both *apo*- and *holo*-CaM bind MARCKS, consistent with the CW-EPR (Fig. S8) and native gels shown in Fig. S9. In these experiments, unlike those with two labels on CaM, there is no contribution to the DEER trace from free CaM, which may be present in solution. A modulation depth of 5-10% was detected for all *holo*-CaM samples and the modulation depth was consistently lower in the absence of calcium, which we attribute to a greater dissociation constant for *apo*-CaM. For CaM T117C and CaM T34C, we observed a narrowing of the distance distribution for *holo*-CaM, whereas the T110C mutant showed no significant differences. The distance distributions remained notably broad also for *holo*-CaM, except for the N60D mutant. This suggests considerable conformational variation in the CaM complex with MARCKS peptide, which does not appear to arise from a distribution of the peptide location as the distance distribution obtained for the N60D-Gd(III) construct was narrow. We also compared the distance distributions with that predicted from the crystal structure using the MMM software(Polyhach et al., 2011) and obtained a reasonable agreement between their maxima (< 0.5 nm difference is comparable to the standard deviation of about 0.3 nm arising from limited accuracy of modelling the distribution of spin label conformations(Jeschke, 2012a)). The predicted widths are, however, consistently narrower than observed, with the difference being particularly large for the T34C mutation in the N-domain of CaM.

The measurements described so far established binding of MARCKS to both *apo*- and *holo*-CaM, yet allowing the N- and C-domain to assume different orientations with respect to each other. Nonetheless, *holo*-CaM in complex with MARCKS showed narrowing of the distance distribution compared to the *apo*-protein, indicating some restriction of the domain locations relative to each other. To further check the degree of agreement between the crystal structure and the solution structure of the Ca^{2+}/CaM/MARCKS complexes we carried out trilateration to determine the position of the MARCKS NO-label as compared to the position predicted by the crystal

structure.(Abdullin et al., 2015) We applied the trilateraton option in the MMM software package(Jeschke, 2018) using Gd(III)–NO mean and standard deviations of the distance distribution in Fig. 4 and the mean position of the Gd(III) ion as determined by the rotamer library, again employing MMM. The results, shown in Fig. S10A, reveal a rather large discrepancy between the location predicted by the crystal structure and the result obtained from trilateration. This further indicates that there are significant differences between the solution and the crystal structures.

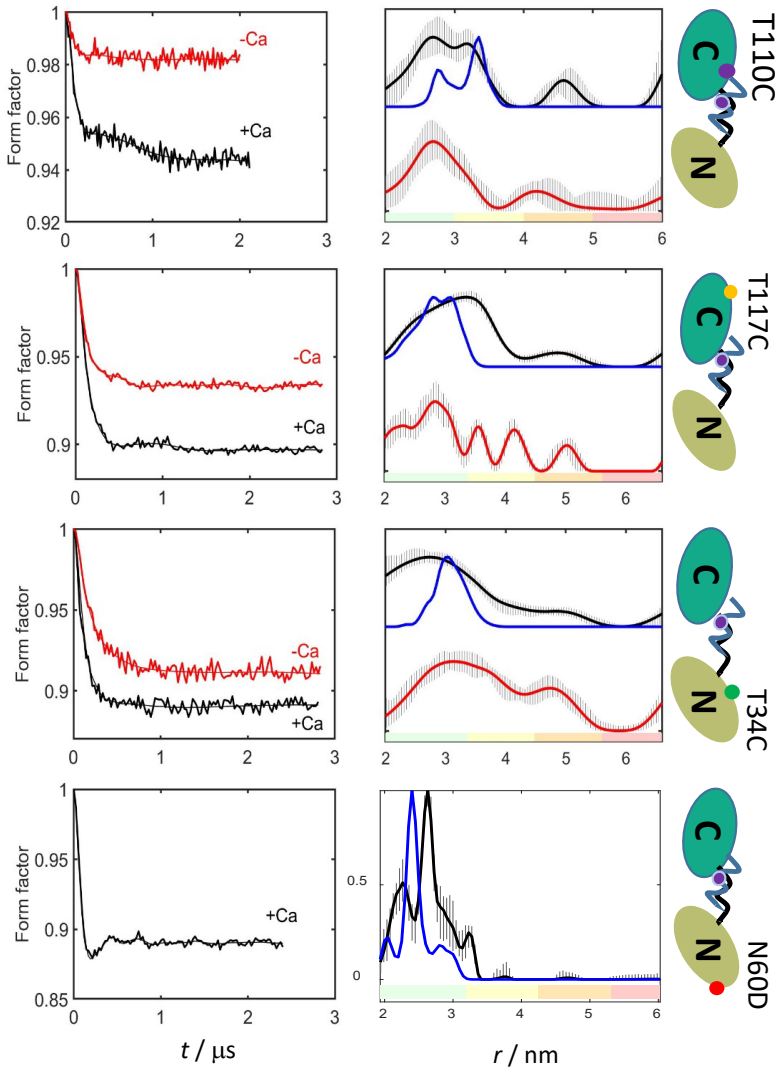

Figure 4. Gd(III)–NO DEER data of *holo*-CaM (black) and *apo*-CaM (red) in the presence of MARCKS. The left column shows the DEER data after background removal with the corresponding fits. The middle column shows the associated distance distributions. Uncertainty ranges are indicated as in Figure 3. The blue line represents the predicted distance distribution from the crystal structure 2BE6, chain A, calculated using the MMM software. The last column shows

cartoons of the CaM/MARCKS complex indicating the labelling scheme. The primary DEER data are given in Fig. S11.

CaM interaction with IQ

To complete the comparison of the CaM-MARCKS and CaM-IQ complexes, we carried out Gd(III)–NO DEER measurements with singly labelled CaM as described above. The IQ peptide was singly labelled with MTSL at two different positions, either towards the C-terminal end (C-IQ) or the N-terminal end (N-IQ; see Methods section and Table 1). According to the crystal structure, the C-IQ label is located near the CaM C-domain, whereas the N-IQ label is closer to the N-domain. The CW EPR spectra of the C-IQ peptide in the presence of different amounts of CaM, shown in Fig. S12, indicated no restriction of motion upon binding to CaM. Fig. 5A shows the Gd(III)–NO DEER results for C-IQ bound to CaM T34C, T110C and T117C mutants labelled with Gd-DOTA-M, in the *apo*- and *holo*-form. In addition, DEER data were acquired for C-IQ and CaM N60D-Gd(III) in the *holo*-state. The results show that the IQ peptide binds CaM both in the absence and presence of calcium, in agreement with earlier reports.(Chagot and Chazin, 2011) For C-IQ, the modulation depths showed little difference between the *apo*- and *holo*-forms (except for the mutant T34C) and the widths of the distance distributions were much greater for CaM T34C and CaM T117C in the *apo*-state. The distance distributions agree reasonably with those predicted for chain A in the crystal structure (except for the mutant T117C), whereas CaM N60D showed a large discrepancy in the width of distance distribution. Although the addition of calcium narrowed the distance distributions, they are broader than anticipated. Fig. 5B presents the results for N-IQ. Again, *holo*-CaM produced narrower distance distributions than *apo*-CaM, particularly for the mutants T110C and T117C, which is consistent with the expectation that binding of the IQ peptides positions the N- and C-domains of CaM in more defined locations relative to each other.(Fallon *et al.*, 2005) Interestingly, the distance distribution width of the CaM N60D-Gd(III)/N-IQ complex is narrower than that with the C-IQ peptide, indicating greater conformational freedom at the C-terminus of the peptide. There was no consistent trend in the modulation depths observed for the *apo*- and *holo*-forms, which may be due to the presence of short distances inaccessible by the experimental set-up of the DEER experiments. The distance distributions of the T117C and T34C mutants matched reasonably the predictions made for chain A, but the mutants T110C and N60D did not match as well, with the T110C and

N60D mutants showing, respectively, somewhat longer and shorter distances than predicted. Regarding chains B and C of the crystal structure, chain B predicts very similar distance distributions as chain A, whereas chain C predicts very different distances (Fig. S13).

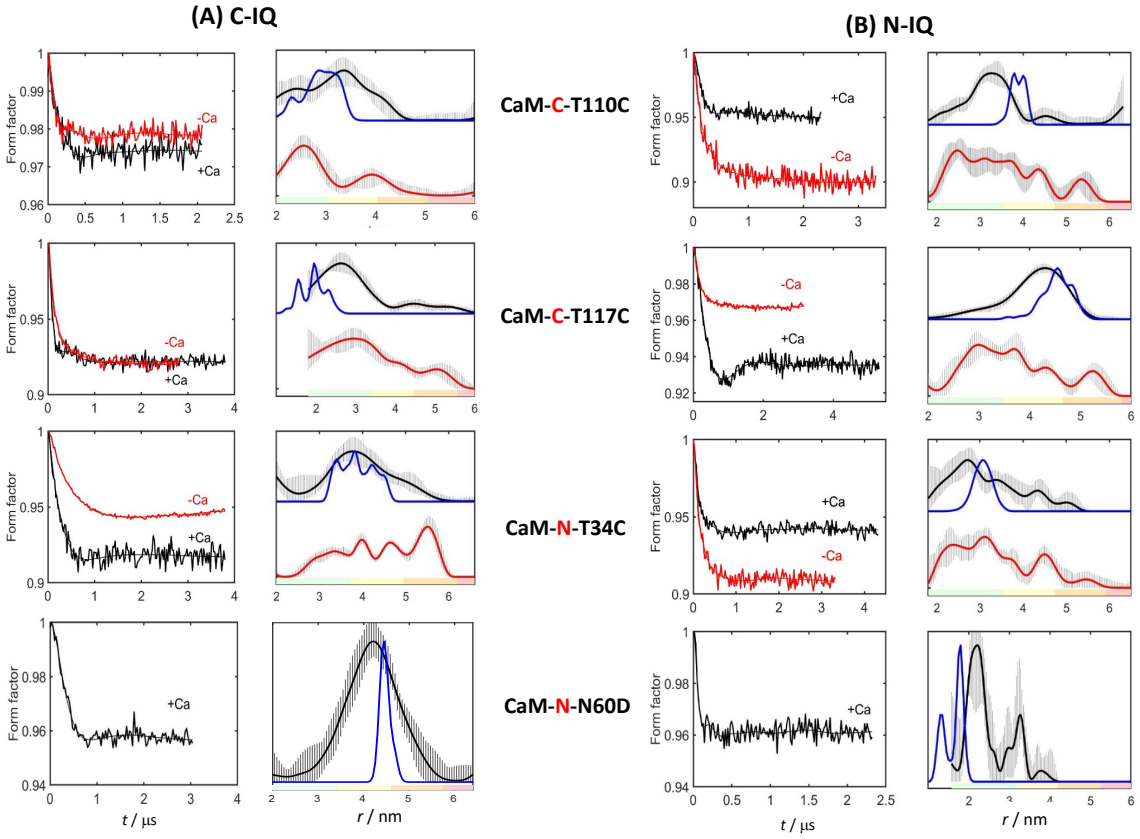

Figure 5. Gd(III)–NO DEER data of *holo*-CaM (black) and *apo*-CaM (red) in the presence of (A) C-IQ or (B) N-IQ peptide. The left column shows the DEER data after background subtraction with the corresponding fits. The middle column shows the associated distance distributions. Uncertainty ranges are indicated as in Figure 3. The blue line represents the predicted distance distribution from the crystal structure 2BE6 (chain A).

DEER measurements were also carried out on IQ labelled with MTSL at both the C- and N-terminal positions in the complex with *holo*-CaM. The distance distribution was again quite broad with a maximum at a shorter distance than predicted (Fig. S14).

We also carried out the trilateration calculation for N-IQ and C-IQ in the Ca^{2+}/CaM/IQ complex, as described above for Ca^{2+}/CaM/MARCKS. Here the agreement was better, showing overlap between the trilateration locations and the cloud of locations predicted from the rotamer library (Fig. S10B,C).

NMR measurements of CaM/MARCKS

PCSs were observed when Tb(III) or Tm(III) ions were added to the CaM N60D mutant. Figure 6 shows the results for both uniformly ^{15}N-labelled CaM N60D and selectively ^{15}N-alanine, ^{15}N-methionine and ^{15}N-valine-labelled CaM N60D loaded with either diamagnetic Y(III) or paramagnetic Tb(III) or Tm(III) in the presence of MARCKS peptide. In total, 28 PCSs were measured for the Tb(III) sample (8 for the N-domain and 20 for the C-domain) and 32 PCSs were measured for the Tm(III) sample (13 for the N-domain and 19 for the C-domain; Table S2).

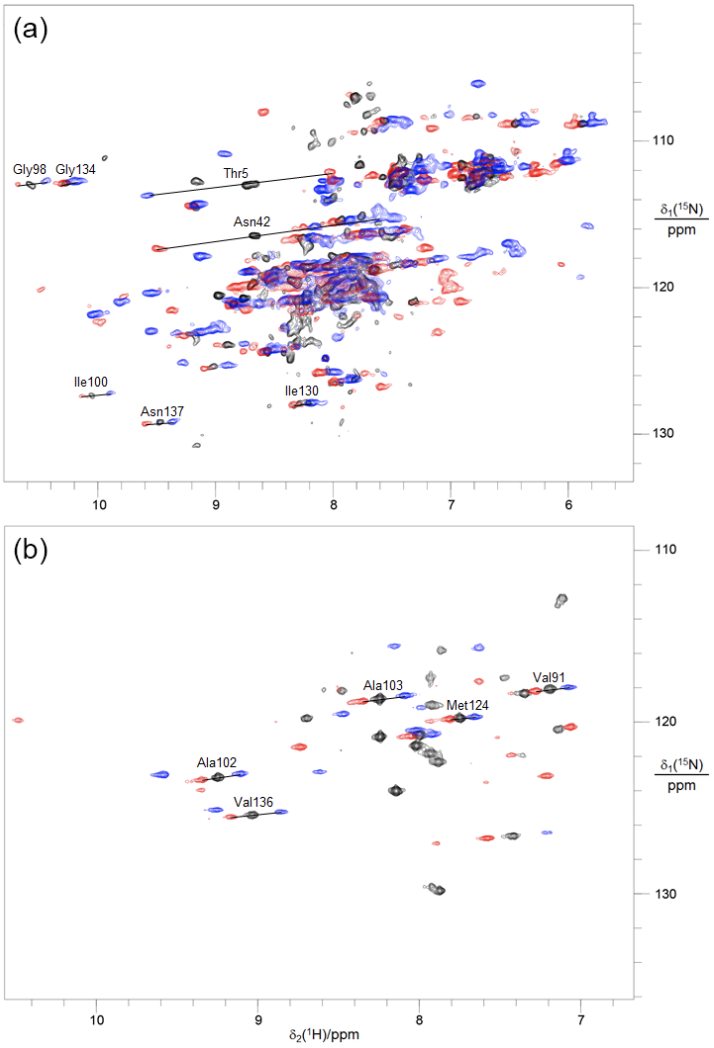

Figure 6. Superimposition of ^{15}N-HSQC spectra of 0.5 mM solutions of CaM N60D with MARCKS peptide. The concentrations of CaM N60D, MARCKS peptide, $CaCl_2$ and $LnCl_3$ were 0.5 mM, 2.5 mM, 1.5 mM and 0.5 mM, respectively. Spectra with diamagnetic Y(III) are in black, and with paramagnetic Tb(III) and Tm(III) in blue and red, respectively. Selected sets of cross-peaks in the diamagnetic and paramagnetic samples are connected by lines and labelled with their resonance assignment. (a) Uniformly ^{15}N-labelled CaM N60D. (b) Selectively ^{15}N-alanine, ^{15}N-methionine and ^{15}N-valine-labelled CaM N60D.

$\Delta\chi$ tensors were determined with the program Numbat,(Schmitz et al., 2008) using the PCSs measured for the N-domain of CaM N60D in complex with MARCKS and Tb(III) or Tm(III), and the crystal structure of the CaM-MARCKS complex 1IWQ (Table S3). The large tensor magnitudes obtained with small quality factors indicate specific binding of the lanthanoid ions with little mobility, as well as excellent agreement with the crystal structure. The magnitude of the $\Delta\chi$-tensor components determined for the CaM N60D/MARCKS complex with Tm(III) are in excellent agreement with the $\Delta\chi$ tensors published for the CaM-DAPK and CaM-DRP-1 complexes(Bertini *et al.*, 2009) and for the CaM-IQ complex.(Russo *et al.*, 2013) This suggests that the N-domain structure is highly conserved between all these complexes. Only the $\Delta\chi_{rh}$ component obtained with Tb(III) is about 50% larger than for the complexes with the other peptides, which may be attributed to the relatively small number of PCSs measured for the N-domain with Tb(III) (Table S2), which may be too small for reliable determination of the $\Delta\chi$-tensor. This conclusion is supported by a direct comparison of the experimental PCSs obtained for the N-domain of the CaM N60D/MARCKS complex with those published previously for the complexes with the DAPK, DRP-1(Bertini *et al.*, 2009) and IQ(Russo *et al.*, 2013) peptides. The correlations were very good (Figure S15). Interestingly, the residues that showed the largest deviations in the correlations (Lys13, Leu18 and Gly23) are located near the hydrophobic pocket of the N-domain which, according to the crystal structure, is almost absent in the CaM-MARCKS complex due to the lack of the anchor residue in MARCKS.(Yamauchi *et al.*, 2003)

The $\Delta\chi$ tensors shown in Table S3 allowed predicting the PCSs for the C-domain as depicted in the crystal structure 1IWQ. Figure 7 shows the correlation between back-calculated and experimental PCSs for both the N- and C-domain. A good correlation between the back-calculated and experimental PCSs was obtained for the N-domain. On the other hand, the correlation between the back-calculated and experimental PCSs for the C-domain was poor with very large quality factors (0.9 for the Tb(III) sample and 1.7 for the Tm(III) sample). The poor fit of the C-domain data indicates that the crystal structure of the CaM/MARCKS complex is not a good representation of the structure in solution. In particular, the experimental PCSs of the C-domain are significantly smaller than expected from the crystal structure. This would be expected, if the distance between N- and C-domain is greater than in the crystal structure. As PCSs depend on the distance *r* from the paramagnetic centre with r^{-3}, the PCSs would decrease two-fold for a 25% increase in distance. In principle, the average PCSs can also decrease, if the C-domain undergoes sideways motions

without changing its distance from the paramagnetic centre located in the N-domain, but it is unclear how such a movement could occur without also increasing the distance between the N- and C-domain.

Figure 8 compares the PCSs reported previously for free CaM N60D(Bertini et al., 2004) with those measured in the present work for the complex with MARCKS peptide. The agreement is good for the PCSs of the N-domain, but the C-domain shows larger PCSs in the complex, indicating that peptide binding reduces the amplitude of motions of the C-domain relative to the N-domain.

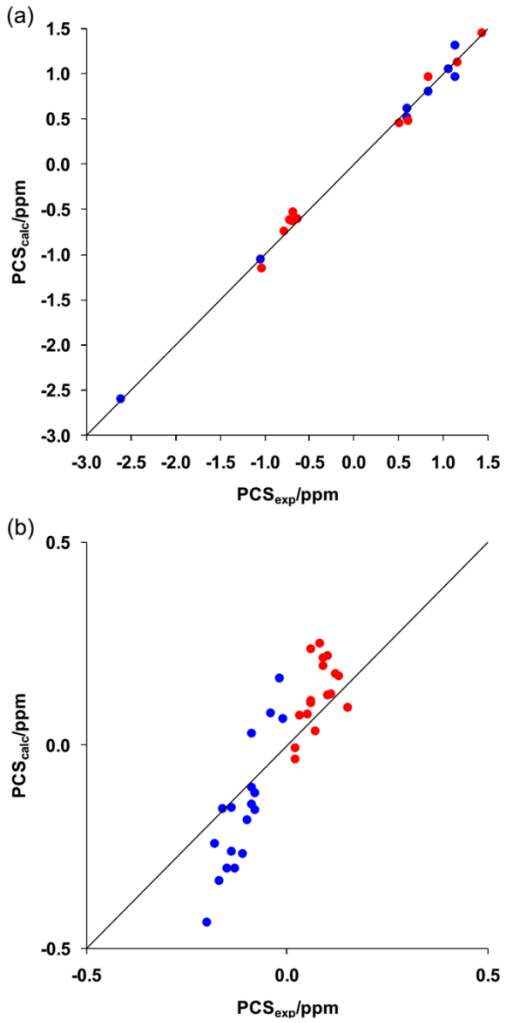

Figure 7. Correlations between back-calculated and experimental PCSs for CaM N60D in complex with MARCKS peptide. (a) Correlation for the amide protons of the N-domain. Blue and red points mark the PCSs obtained with Tb(III) and Tm(III), respectively. (b) Same as (a) but for the C-domain.

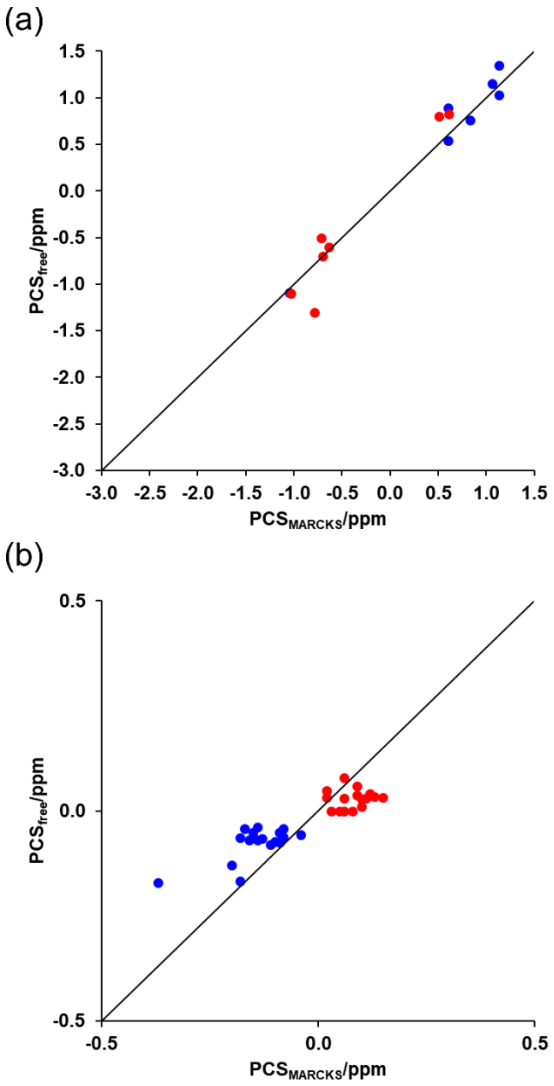

Figure 8. Correlations between experimental PCSs measured for free *holo*-CaM N60D(Bertini *et al.*, 2004)and CaM N60D in complex with MARCKS peptide. (a) Correlation for the amide protons of the N-domain. Blue and red points mark the PCSs obtained with Tb(III) and Tm(III), respectively. (b) Same as (a) but for the C-domain.

Modelling of the solution structure of holo-CaM/IQ

Comparing the collection of DEER distance distributions measured for the *holo*-CaM/IQ complex with those predicted from the crystal structure for chains A and B(Fallon *et al.*, 2005) suggests that the average solution structure is not very different but it is also characterized by significant conformational heterogeneity as also observed by NMR.(Russo *et al.*, 2013) Using the elastic-network model implemented in MMM,(Jeschke, 2012a; Jeschke, 2018) we constructed a model

of the *holo*-CaM/IQ complex based on the DEER restraints, adopting the approach taken to model the conformational change in hyperpolarization-activated cyclic nucleotide-gated (HCN) carboxyl-terminal region upon binding of cyclic AMP.(Puljung et al., 2014) The modelling aimed to derive a family of structures that are consistent with the DEER distance distributions and reflect the solution structure. The crystal structure of chain A was taken as the initial model and the 12 experimental distance distributions were converted into 12 structure restraints. The distance distribution obtained with N60D-Gd(III)-T117-MA-proxyl gave a bimodal distribution hinting at the presence of two conformations. Therefore, we considered three restraint cases for this variant, one with a short distance, another with a long distance and a third with their average, as listed in Table S4. The fit was performed 20 times for each set of restraints, generating three ensembles of structures, depicted in Fig. 9 for two different views of the protein/IQ complex. The average r.m.s.d. values and the standard deviation (in parenthesis) obtained for the average, long and short sets of restraints were rather small, 2.07 (0.412), 2.03 (0.107) and 2.10 (0.14) Å, respectively. We calculated the average distance distributions derived from these three structure ensembles using MMM and compared them to the experimental results for the long restraint case in Fig. 10 and the results obtained for the other two cases are shown in Fig. S16. The sum of the squares of the differences between the maxima of the experimental distance distributions and the distance distributions calculated for the new structures show that the match is better for the short and long distance cases than for the average distance case (Fig. S17). None of the three sets reproduced the short distance observed for the N60D-Gd(III)-T117-MA-proxyl construct. Regarding the overall fold of the protein, the differences between the three structures shown in Fig. 9 are relatively minor, with movements in all helices compared to the crystal structure (chain A) and the C-terminal segment of the IQ peptide showing significant disorder. The N-terminal segment of the IQ peptide is disordered too, but less so. The central region of the peptide shows the least disorder for the case when the short restraint was used. Significant disorder was observed also for the second EF hand of the N-terminal domain, which binds the Gd(III) ion in the N60D mutant and suggesting an averaged small shift.

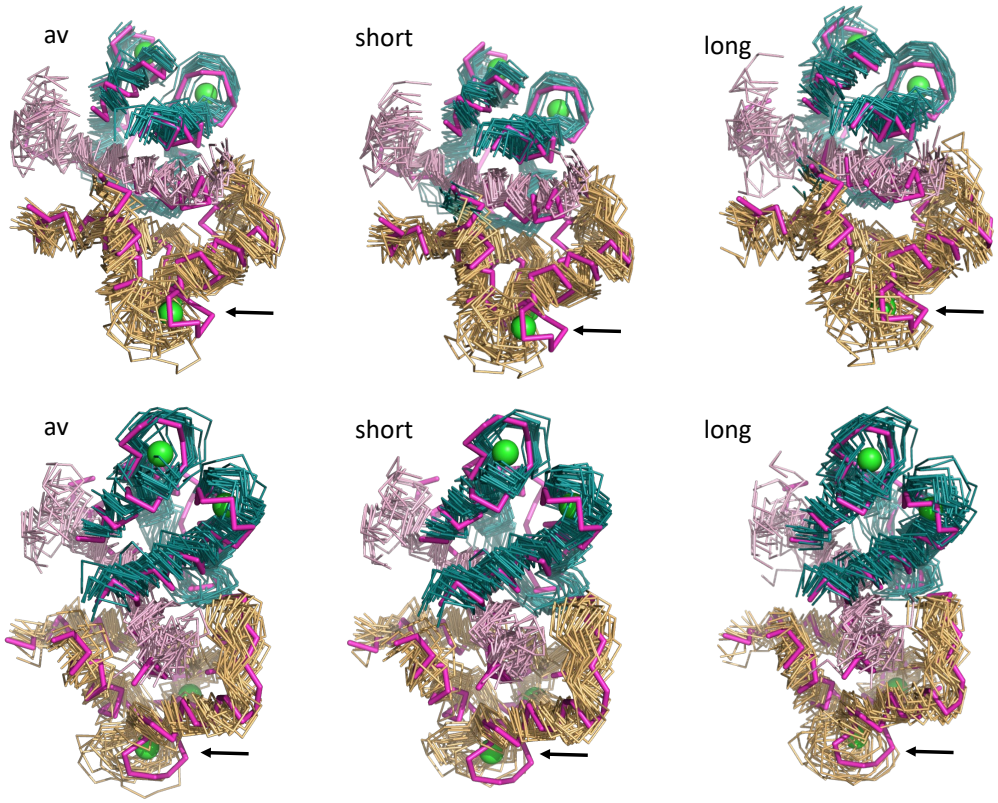

Figure 9. Two views of the ensemble of 20 structures obtained from fitting the distance distributions using the elastic network model and the experimental results of all constructs of *holo*-CaM in complex with IQ peptide as restraints (twelve in total). The calculations were performed by setting the restraints obtained with *holo*-CaM T117C-Ma-proxy/N60D-Gd(III) either to average (av), short or long distances. The magenta ribbon corresponds to the A chain in crystal structure 2BE6. The Ca^{2+} ions are shown as green balls. The position of the Gd(III) ion in the N60D mutant is identified by an arrow. The IQ peptide is shown in pink, the N-domain in gold, and the C-domain in deep teal.

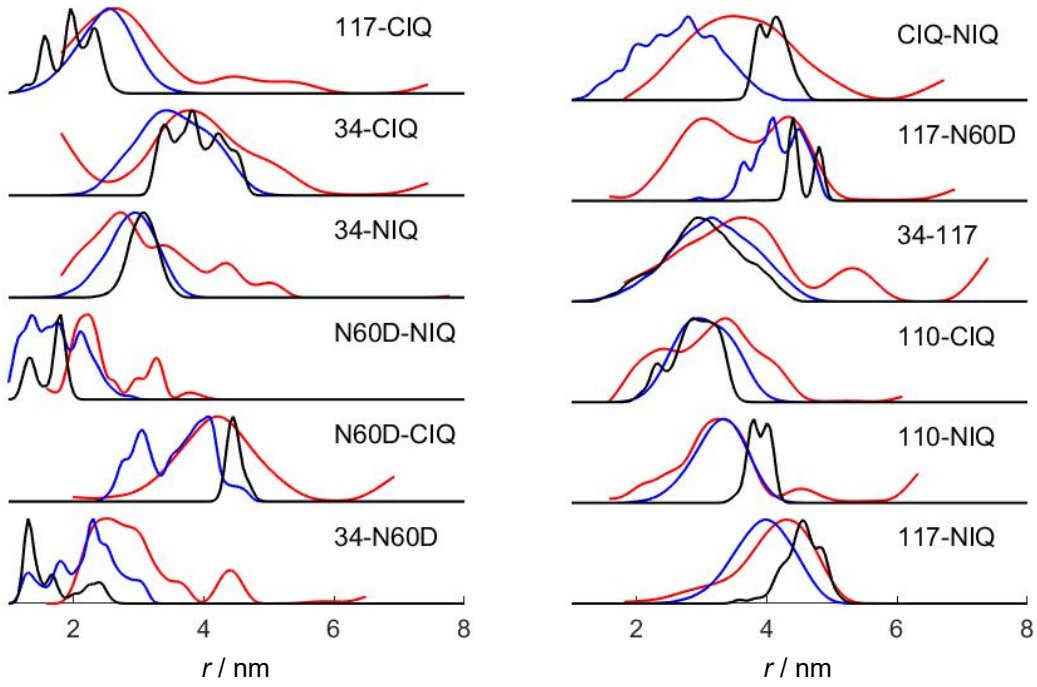

Figure 10. Comparison of the distance distributions in the structures fitted with the long distance restraint option (blue), distance distributions modelled on the X-ray structure (black) and the experimental results (red) for all constructs of *holo*-CaM. The T117C-MA-proxyl/N60D-Gd(III) construct shows a second distribution with a short distance, which is not accounted for by either the model or crystal structure.

Discussion

In this work, we used DEER with various labelling schemes, combining different Gd(III) and nitroxide labels, and paramagnetic NMR measurements to explore the solution structure of CaM in the presence of two target peptides, MARCKS and IQ, which belong to different families of proteins. Although the co-crystal structures with both peptides exhibit a closed structure (Fig.1), the detailed binding modes of the peptides differ. Our attempt to resolve the manifestation of these differences in solution followed two approaches. In the first we looked for the conformational changes that *holo*-CaM undergoes upon peptide binding by tracking the distance distributions between pairs of labels on CaM. In the second approach we focused on the interaction between the peptide and CaM by measuring distance distributions between a spin label on the peptide and another on CaM. Our experimental observations can be summarized as follows: (i) CaM binds the MARCKS and IQ peptide both in the *apo*- and *holo*-states. The binding

affinity for MARCKS is lower in the *apo*- than *holo*-state. (ii) Upon binding of the MARCKS peptide, *holo*-CaM does not predominantly assume the closed conformation observed in the co-crystal structure but retains the structure of the N-domain, whereas the complex with the IQ peptide is reasonably represented by the co-crystal structure. (iii) Both *holo*-CaM/IQ and *holo*-CaM/MARCKS complexes retain significant structural disorder, with the complex with the MARCKS displaying greater disorder. (iv)Using a dozen DEER distance restraints for the *holo*-CaM/IQ complex, application of the elastic network model allowed us to derive a structure from the crystal structure that is compatible with the solution data. Beyond some movement of all helices around the crystal structure, the main differences observed pertained to the disorder of the N- and C-terminal segments of the IQ peptide and some disorder of the Gd(III) ion located in the second EF hand of the N-domain in the N60D mutant accompanied by a small shift in its average position. It is interesting to discuss the implications of these observations in terms of the effect of peptide binding on the conformational space of CaM.

To begin with, the DEER data obtained were in satisfactory agreement with the formation of a closed structure as described by the *holo*-CaM/IQ crystal structure. CaM labelled both in the C-domain (T117C) and N-domain (T34C) showed a significant shortening of the distance and narrowing of the distance distribution upon binding the IQ peptide(Dalaloyan *et al.*, 2019), in close agreement with the predictions made from all conformations reported in the crystal structure.. The width of the distance distribution for this particular mutant was also in good agreement with the predictions, indicating that it arises primarily from the flexibility of the tether of the Gd(III)-DOTA-M tag. Unexpectedly, however, CaM N60D-Gd(III)-T117C–MA-proxyl showed a bimodal distribution, where the longer distance is in agreement with the prediction based on the crystal structure. The shorter distance may correspond to a second conformation of the N60D-Gd(III) binding loop, but in this case bimodal distributions would be expected for all CaM N60D-Gd(III) constructs. A second, albeit weaker peak was indeed observed in the distance distributions of CaM N60D-Gd(III)/T34C-MA-proxyl and CaM N60D-Gd(III)/N-IQ. In the complex CaM N60D-Gd(III)/C-IQ the distance distribution was very broad, which may prevent the resolution of the two distance distributions. While the possibility of a second conformation cannot be excluded, it would mean quite a large shift of 1.5 nm in the Gd(III) position. The paramagnetic NMR measurements do not support this, as the correlation between experimental and calculated PCSs was good for the N-domain in the complex with MARCKS and the PCSs also correlated well with those observed in the *holo*-CaM/IQ complex. Another possible explanation could be the presence

of a second set of conformations of the MA-proxyl label at the site T117C, which is not picked up by the rotamer library, or a second orientation of the G helix, but these explanations are not supported by a resolved bimodal distribution of any other construct with T117C and IQ peptide.

The IQ peptide was found to bind also to *apo*-CaM. In this case, the distance distributions were generally significantly broader than for the *holo*-state, consistent with the NMR structure.(Chagot and Chazin, 2011) This allows high flexibility of the N-terminal segment of the peptide and of the CaM N-domain relative to the C-domain. The distance distributions narrow significantly in the presence of calcium and in general the distance distributions are in reasonable agreement with those predicted from the crystal structure, in particular chain A. Nonetheless, the distance distributions predicted were generally narrower than the experimental ones, suggesting the presence of significant protein flexibility also in the closed state.

Use of the elastic network model generated an ensemble model of *holo*-CaM/IQ in agreement with the experimentally determined DEER distance restraints, indicating the existence of disorder in the frozen solution. Particular disorder was noted for the IQ peptide labelled near its C-terminus, consistent with the high mobility reflected in the corresponding CW EPR spectra, while the disorder was lower for the IQ peptide labelled near the N-terminus. The conformers generated by the elastic network model indicated that the central helical part of the peptide remains fairly ordered. The Gd(III) ion in the second EF hand of the N-domain showed greater displacements compared to the calcium sites, with different average positions of the Gd(III) ion obtained in the short and long restraint cases. While the N60D mutation together with binding of a trivalent ion could cause a structural perturbation, earlier NMR studies indicated that this substitution preserves the structure.(Bertini *et al.*, 2009) A recent 2D IR study reported that, relative to the calcium-loaded form, CaM exhibits greater conformational flexibility when loaded with lanthanide ions including larger structural fluctuations within their binding sites. In this study, however, all four calcium ions were substituted.(Edington et al., 2018) In addition to the short distance observed for N60D-Gd(III)-T117C–MA-proxyl, which was not reproduced by the elastic network fit, the distance distribution obtained between the two labelling sites in the N-IQ and C-IQ peptides could not be fitted by any of the restraint sets used, as all models underestimated this distance. It is important to note, however, that the fits produced by the elastic network model heavily rely on determining the positions of the Gd(III) ion and NO radical through rotamer libraries, which have their own uncertainties of 0.2-0.3 nm.(Jeschke, 2012a)

While the calcium-to-Gd(III) substitution in the N60D mutant was designed to reduce the dependence on rotamer libraries and the modelled structures generally match the experimental data, some discrepancies remain in particular for the N60D-Gd(III) constructs. In the case of the N60D-Gd(III)-T34C and N60D-Gd(III)-N-IQ constructs, discrepancies could arise from the experimental difficulty to access very short distances by DEER.

The DEER data of the CaM/MARCKS complex did not yield sufficient good quality restraints to carry out a structure analysis with the elastic network model. The data obtained with the IQ peptide serve as a helpful reference for the more complex behaviour of the MARCKS peptide and for establishing that any failure to detect the closure of the N- and C-domains upon binding of MARCKS is not an artifact of spin-labelling. All DEER measurements on the CaM/MARCKS complex with labels positioned in the N- and C-domain (11 pairs), except for the mutant N53C/E119C, gave broad distance distributions for *holo*-CaM with and without MARCKS, showing only minor differences between the two. This behaviour is consistent with MARCKS binding firmly only to one of the two domains, leaving the two domains free to assume a range of different orientations relative to each other. The widths of the distance distributions between labelled *holo*-CaM and labelled peptide were similar to those of *holo*-CaM/IQ, despite the MARCKS peptide being labelled in the centre of the helix, where the label motion would be expected to be highly restricted, while the IQ peptide was labelled closer to its termini, where the labels are conformationally less restricted. This is again consistent with preferred binding of MARCKS to only one of the CaM domains. NMR measurements performed with CaM N60D loaded with paramagnetic lanthanoid ions and in complex with MARCKS peptide yielded PCSs of the C-domain that were significantly smaller than expected for the co-crystal structure 1IWQ, but larger than in the free protein. This situation is reminiscent of the complex between *holo*-CaM N60D and the small intrinsically disordered protein AS, where the domains of CaM are somewhat more ordered in the complex with AS than in the free protein, but still show significant disorder in their relative orientation.(Bertini et al., 2007) Most notably, the PCSs of the N-domain clearly support the notion that the N-domain retains its structure in the N60D mutant as observed in the crystal structure 1IWQ. The conservation of the N-domain structure indicated by the NMR data also suggests that the apparent movement of the Gd(III) ion in the lanthanoid ion binding loop of CaM/IQ requires a different explanation such as the short distance limitation of the DEER

measurements. Finally, the MARCKS peptide in the crystal structure is shorter than the MARCKS peptide used in the present work, raising the possibility that peptides of different lengths bind in different ways and stressing the importance of future studies of the full length target proteins.

Conclusions

By employing several labelling schemes and using different Gd(III) and nitroxide spin labels, W-band DEER measurements of Gd(III)–Gd(III), Gd(III)–nitroxide and nitroxide–nitroxide distances provided clear evidence for binding the target peptides MARCKS and IQ to CaM both in its *apo*- and *holo*-states. In the *holo*-state the two peptides revealed different behaviours, which were not expected based on the available crystal structures. Binding of the MARCKS peptide does not produce the closed conformation reported by the crystal structure as the main conformational species. Instead, the relative orientations of the N- and C-domains remain highly variable as also confirmed by complementary paramagnetic NMR measurements. In contrast, binding of the IQ peptide to *holo*-CaM generated a closed conformation as expected, albeit with greater conformational heterogeneity than suggested by the crystal structure. With the input of twelve distance restraints derived from the combined DEER data of the *holo*-CaM/IQ complex, the elastic network model enabled the construction of a model of the solution structure that is close to the crystal structure. This structural model suggests high flexibility of the N- and C-terminal segments of the IQ peptide and a potential structural distortion of the Gd(III) binding site in the Gd(III)-N60D mutant. Finally, the holistic DEER approach used can be applied in the future to study CaM interaction with full length partners, as opposed to small peptides, which may not show the full picture.

Materials and methods:

CaM Expression and Purification

The wild-type gene (AAD45181.1) of human CaM was cloned into the pETMCSI vector(Neylon et al., 2000) with an N-terminal His_6 tag followed by a tobacco etch virus (TEV) protease recognition site. To study the complex with MARCKS, nine CaM mutants were produced with two cysteine residues at specific positions for labelling with Gd(III) tags (Table S1). The proteins were produced by cell-free protein synthesis from PCR-amplified DNA.(Wu et al., 2007) Each cell-free reaction

was conducted at 30 °C for 16 h in a dialysis system with 3 mL inner reaction mixture and 30 mL outer buffer following a published protocol.(Otting, 2008)

The proteins were purified using a 1 mL Ni-NTA column (GE Healthcare, USA) according to the manufacturer's protocol. Afterwards, the N-terminal His_6 tag was removed by incubation with His_6-tagged TEV protease(Cabrita et al., 2007) at 4 °C for 16 h in a buffer of 25 mM Tris-HCl, pH 8, 500 mM sodium chloride and 2 mM 2-mercaptoethanol (BME). CaM was separated from the cleaved His_6 tag and the TEV protease by running the mixture again over a Ni-NTA column. Finally, the protein samples were dialyzed against 50 mM sodium phosphate, pH 8, at 4 °C and then concentrated using an Amicon ultrafiltration centrifugal tube with a molecular weight cutoff of 5 kDa. The average yield was about 2 mg of purified protein per mL cell-free reaction mixture (inner buffer). The protein concentrations were confirmed by UV absorption measurements and the bicinchoninic acid assay.(Smith et al., 1985) Both measurements agreed within 10%.

In addition, the four CaM single-point mutations N60D, T117C, T34C and T110C and three double mutants (T117C/T34C, T117C/N60D, T34C/N60D) were prepared to study both the CaM/MARCKS and CaM/IQ complex. These mutants were expressed with a His_6 tag from a pET28 plasmid in *E. coli* BL21(DE3) cells. Following cell harvesting by centrifugation and cell lysis by sonication in the presence of protease inhibitors and DNase, the cell debris was removed by centrifugation. Further purification of the supernatant was conducted using a HisTrap Crude Ni-NTA column followed by a HiTrap HP ion exchange column and a Superdex size exclusion column. Finally, the buffer was exchanged to 20 mM Tris-HCl, 50 mM KCl and 5 mM BME, pH 7. For all mutants, each purification step was monitored by 15% SDS-PAGE. Fig. S18 shows the results obtained for all mutants. The final protein concentration was determined by UV-Vis at 280 nm.

Peptides

The MARCKS peptide comprised residues 151–175 (KKKKKRFSFKKSFKLSGFSFKKNKK) of myristoylated alanine-rich protein kinase C substrate.(Glaser et al., 1996) The peptide was purchased from AnaSpec (Fremont, CA) and GenScript (Piscataway, NJ). MARCKS and its mutant K164C were purchased from ProteoGenix (Schiltigheim, France). The amino acid sequence of the MARCKS peptide used in our study was the same as used in earlier NMR and EPR studies.(Porumb et al., 1997b; Qin *et al.*, 1996) In contrast, the peptide used in the crystal structure 1IWQ was shorter (KKRFSFKKSFKLSGFSF).(Yamauchi *et al.*, 2003). (Note that the sequence numbering in the crystal structure differs, with K154 in our

sequence corresponding to K148 in the crystal structure.) The IQ peptide comprised residues 1608–1644 (GHMDEVTVGKFYATFLIQEYFRKFKKRKEQGLVGKPS) from the voltage-gated Ca Channel Ca(V1.2). The wild-type peptide and its mutants V1615C and V1640C were purchased from ProteoGenix (Schiltigheim, France).

Spin labelling

Labelling with C1 tag: Prior to ligation with the C1 tag (**Error! Reference source not found.**), 0.1 mM CaM solutions in 50 mM sodium phosphate, pH 8, were reduced with 5 mM dithiothreitol (DTT) and the DTT was removed using an Amicon ultrafiltration centrifugal tube. The reduced protein solution was added slowly into a solution of 5 molar equivalents of C1-Gd(III) in the same buffer and kept overnight at room temperature. Complete tagging of the samples was confirmed using mass spectrometry. After the tagging reaction, the protein samples were concentrated and exchanged to EPR buffer 1 (20 mM Tris-HCl, 200 mM KCl in D_2O, pD 8.8, uncorrected pH meter reading) using an Amicon ultrafiltration centrifugal tube, and perdeuterated glycerol was added to a final concentration of 20% (v/v). The high concentration of KCl served to minimize protein dimerization.(Lafitte *et al.*, 1999a)

Labelling with Gd(III)-DOTA-maleimide (DOTA-M) tag: All three single mutants (T34C, T110C and T117C) and the double mutant T34C/T117C were labelled with Gd-DOTA-M as described earlier(Dalaloyan *et al.*, 2019; Martorana et al., 2014). We first loaded DOTA-M (purchased from Macrocyclics) with gadolinium by dissolving $GdCl_3$ and DOTA-M in distilled water at a molar ratio of 1.2:1 and adjusting the pH to 5.5–6.0 by slow addition of 0.1 M NaOH. The solution was mixed at room temperature for 3 h and subsequently lyophilized.

The protein was treated with 20 mM dithiothreitol (DTT) and kept on ice for 15 minutes. DTT and BME were removed from the protein solution using a PD-10 column. The reduced protein eluted from the column was added to a solution of Gd-DOTA-M dissolved in 500 µL anhydrous DMF (final molar ratio protein:tag = 1:5 and a total volume of 3 ml, 17% DMF). The mixture was incubated at room temperature for 4 h in argon atmosphere under gentle stirring. The solution was again lyophilized and DMF is removed before size exclusion chromatography in order to remove

unbound tag and excess Gd(III). The correct fold of the protein was established by CD measurements.

The N60D mutant was loaded with gadolinium by treating the protein for 10 min with an equimolar ratio of $GdCl_3$ solution in EPR working buffer 2 (20 mM MES 200 mM KCl, pH 6.5).

After the tagging reaction, the protein samples were concentrated and exchanged to EPR buffer using an Amicon ultrafiltration centrifugal tube and perdeuterated glycerol was added to a final concentration of 20% (v/v). The final protein concentration was 0.1–0.2 μM.

3-Maleimido-PROXYL labelling: T117C/N60D and T34C/N60D were labelled with 3-maleimido-proxyl (MA-proxyl, obtained from Sigma). The protein, in 20 mM Tris-HCl, 50 mM KCl, pH 7, was mixed with the tag in 1:10 molar ratio at room temperature for 3 hours. Excess tag was removed using a Biospin column and labelled protein was concentrated using a 5 kDa cut-off vivaspin concentrator. Finally, the buffer was exchanged to EPR working buffer and perdeuterated glycerol was added to a final concentration of 20% (v/v). The final protein concentration was 0.1–0.2μM.

Peptide labelling: Prior to labelling, the V1615C and V1640C mutants of the IQ peptide and the MARCKS K164C peptide were treated with 20 mM DTT, keeping the solution on ice for 15 minutes, and excess DTT was removed by a semi-preparative HPLC column (ZORBAX C18, 5μm, 9.4X250mm) using an acetonitrile-water gradient. The reduced fraction was collected and labelled by adding MTSL (*S*-(1-oxyl-2,2,5,5-tetramethyl-2,5-dihydro-1H-pyrrol-3-yl)methyl methane-sulfonothioate, purchased from Sigma-Aldrich) immediately in ten-fold molar excess. The mixture was incubated overnight at 4 °C, excess MTSL was removed using the same HPLC column, and an acetonitrile-water gradient (10–100% in 50 minutes for the IQ peptides and 30 minutes for the MARCKS peptide). The labelled peptide fraction was collected and concentrated in a SpeedVac rotor concentrator removing the acetonitrile. Finally the concentrated labelled peptide was diluted in EPR working buffer as needed for the measurements. Table 1 lists all the constructs prepared, excluding those listed in Table S1, and the DEER distance measurements they were subjected to.

The nitroxide labelling efficiencies were determined by X-band CW-EPR spectra. For Gd(III) labelling, the labelling efficiency was estimated by comparing the echo intensities with a solution of $GdCl_3$ considering the differences in the width of the signal. Labelling efficiencies were 60–70% for the CaM single mutants except T110C, where it was 50%. For the double mutants T117C/N60D and T34C/N60D the efficiency was 50% and 35% respectively. For C-IQ and MARCKS the efficiency was 100%, as labelled and unlabelled peptides were separated using HPLC.

Table 1. Summary of CaM constructs prepared, the corresponding labels and the label pair subjected to DEER measurements. C1-labelled CaM samples are listed in Table S1.

#	Mutant	Domain /helix	Label 1	mutation	Domain/helix	Label2	DEER
1	T117C	C/G*	Gd-DOTA-M	T34C	N/B	Gd-DOTA-M	Gd(III)–Gd(III)
2	T117C	C/G*	MA-proxyl	N60D	N/ between C,D	Gd(III)	Gd(III)–NO
3	T34C	N/B	MA-proxyl	N60D	N/ between C,D	Gd(III)	Gd(III)–NO
4	T117C	C/G*	Gd-DOTA-M	IQ, N-term	peptide	MTSL	Gd(III)–NO
5	T117C	C/G*	Gd-DOTA-M	IQ, C-term	peptide	MTSL	Gd(III)–NO
6	T117C	C/G*	Gd-DOTA-M	MARCKS K164C	peptide	MTSL	Gd(III)–NO
7	T34C	N/B	Gd-DOTA-M	IQ, N-term	peptide	MTSL	Gd(III)–NO
8	T34C	N/B	Gd-DOTA-M	IQ, C-term	peptide	MTSL	Gd(III)–NO
9	T34C	N/B	Gd-DOTA-M	MARCKS K164C	peptide	MTSL	Gd(III)–NO
10	T110C	C/F	Gd-DOTA-M	IQ, N-term	peptide	MTSL	Gd(III)–NO
11	T110C	C/F	Gd-DOTA-M	IQ, C-term	peptide	MTSL	Gd(III)–NO
12	T110C	C/F	Gd-DOTA-M	MARCKS K164C	peptide	MTSL	Gd(III)–NO
13	N60D	N/between C,D	Gd(III)	IQ, N-term	peptide	MTSL	Gd(III)–NO

14	N60D	N/between C,D	Gd(III)	IQ, C-term	peptide	MTSL	Gd(III)–NO
15	N60D	N/between C,D	Gd(III)	MARCKS K164C	peptide	MTSL	Gd(III)–NO

* Immediately before the start of helix G.

Protein/peptide complexes

The nine double mutants listed in Table S1 and labelled with C1 were studied in the presence and absence of MARCKS. The peptide was added in excess, with a peptide:CaM ratio of 4:1. Peptide (1 µL, 1 mM) was added to CaM (2.5 µL, 100 µM), both in 20 mM Tris-HCl in D_2O, pD 8.8, 20% glycerol-d_8, 0.5 mM $CaCl_2$ and 200 mM KCl, followed by 5 minutes incubation on ice. All final samples contained 70 µM CaM. Sample volumes of about 3 µL were loaded into 0.6 mm ID, 0.84 mm OD quartz capillaries from Vitrocom, flash frozen in liquid nitrogen and kept frozen. All measurements were carried out on frozen solutions. All other protein-peptide complexes were studied in the presence (5 mM $CaCl_2$) and absence of calcium (3 mM EDTA was added into the solution to remove any Ca^{2+} ions). The peptide:CaM ratio used was 1:1, each at 50 µM final concentration. The peptide and CaM, both in 20 mM MES, 200 mM KCl in D_2O, pH 6.5, 20% glycerol-d_8, 5 mM $CaCl_2$ were mixed and incubated for 5 minutes on ice. The samples containing two Gd-DOTA-M tags were prepared with 100 mM $CaCl_2$, whereas the N60D mutants containing a Ca^{2+} to Gd^{3+} substitution contained 5 mM $CaCl_2$ and 50 µM $GdCl_3$. The binding of the MARCKS peptide to *apo*- and *holo*-CaM was confirmed by native gels (Fig. S9). Sample volumes of about 3 µL were loaded into 0.6 mm ID, 0.84 mm OD quartz capillaries (Vitrocom, USA), flash frozen in liquid nitrogen and kept frozen. All measurements were carried out on frozen solutions.

NMR sample preparation

The CaM N60D mutant was cloned into the pETMCSI vector and the plasmid was transformed into *E. coli* BL21(DE3) cells. Uniformly ^{15}N- or $^{13}C/^{15}N$-labelled samples were prepared by inoculating 1 L of LB medium containing 100 µg/mL ampicillin with 10 mL of an overnight culture. After growing to an OD_{600} of 0.8, the cultures were changed to 500 mL minimal medium containing 0.1% $^{15}NH_4Cl$ as the sole nitrogen source, or 1% [U-^{13}C]-glucose and 0.1% $^{15}NH_4Cl$ as the sole carbon and nitrogen sources. Following incubation at 37 °C for another 1–2 h, overexpression was induced

with 1 mM isopropyl-β-D-thiogalactopyranoside (IPTG). The cultures were harvested after overnight expression (about 16 h) at 25 °C by centrifugation. Pellets were resuspended in buffer A (20 mM HEPES buffer, pH 7.5, 300 mM NaCl, 5% glycerol, 20 mM imidazole) and the cells were lysed using a French press at 12,000 psi. The cell lysates were centrifuged for 1 h at 34,000 *g*. The supernatant was loaded onto a 5 mL Ni-NTA column (GE Healthcare, USA) and the protein was eluted with buffer B (same as buffer A but containing 500 mM imidazole). The fractions were analyzed by 12% SDS-PAGE. Fractions containing protein were pooled and the N-terminal His_6 tag was removed by incubation with TEV protease as mentioned before. Finally, the protein samples were dialyzed against NMR buffer (30 mM HEPES buffer, pH 6.8, 200 mM KCl) at 4 °C and then concentrated using an Amicon ultrafiltration centrifugal tube. In addition, a CaM N60D sample selectively labelled with ^{15}N-alanine, ^{15}N-methionine and ^{15}N-valine was prepared for PCS measurement. The same cell-free protocol was used as described above,(Otting, 2008) except that each cell-free reaction was conducted with 2 mL inner reaction mixture and 20 mL outer buffer with 1 mM ^{15}N-alanine, ^{15}N-methionine and ^{15}N-valine present in both inner and outer buffers.

EPR Spectroscopic measurements

(a) CW-EPR measurements

All CW-EPR measurements were carried out on an X-Band (9.4 GHz) Bruker E500 spectrometer using quartz capillaries of 0.84 mm o.d. and 0.6 mm i.d. at room temperature. Measurement parameters: modulation amplitude, 1.000 G; conversion time, 40ms; sweep time, 20.48 s; sweep width, 10 mT.

Pulsed-EPR measurements

All pulsed EPR measurements were carried out on a home built W-Band (95GHz) spectrometer(Goldfarb et al., 2008) equipped with an arbitrary waveform generator (AWG). (Bahrenberg et al., 2017)Echo-detected EPR (ED-EPR) spectra were recorded using the $\pi/2$-τ-π-τ-echo sequence, with a two-step phase cycle (0,π) on the first $\pi/2$ pulse, while holding τ fixed and sweeping the magnetic field. The experimental parameters for observing Gd(III) and nitroxide signals are given in Table 2.

Table 2. Experimental parameters used to record ED-EPR spectra.

Parameters	**Nitroxide**	**Gd(III)**
Temperature	50 K	10 K
π/2-π	15–30 ns	15–30 ns
τ	600 ns	600 ns
Repetition time	2 ms	1 ms

DEER measurements employed the standard four pulse DEER sequence, ($\pi/2_{vobs} - \tau_1 - \pi_{vobs} - (\tau_1+t) - \pi_{vpump} - (\tau_2-t) - \pi_{vobs} - \tau_2 -$ echo),(Pannier et al., 2000) using either a rectangular or chirp pump pulse monitoring the echo intensity with increasing delay *t*. An eight-step phase cycling was applied unless stated otherwise. Accumulation times were between 5 and 22 h, depending on the evolution time and the signal-to-noise ratio.

Gd(III)–Gd(III) DEER: The C1-labelled samples were measured with pulse durations of $t_{\pi/2,\pi}$ (obs) = 15, 30 ns, t_{pump} = 15 ns and a four-step phase cycle for the observe pulses, τ = 350 ns and a repetition time of 0.8 ms. The pump frequency was set to the maximum of the Gd(III) spectrum and the observe frequency was 120 MHz higher. The echo was measured as a function of *t*, which was incremented from an initial value of about -200 ns in steps ranging from 25 to 50 ns, depending on the observed distance. The evolution time *T* was between 3 and 6 μs, depending on the distance, and the number of steps for the *t* increment was determined accordingly.

All other Gd(III)–Gd(III) DEER used chirp pump pulses with a duration of 128 ns set to the central transition to cover the range 94.925–95.075 GHz (150 MHz bandwidth) and the observe pulses were set to 94.85 GHz with pulse durations π/2,π = 15,30ns. The maximum of the Gd(III) signal was set to 95 GHz. The repetition rate was 200 μs and the accumulation time was 5–22 h depending on the sample and the temperature was 10 K.

Gd–NO DEER**:** The resonator was first tuned at 94.9 GHz and the magnetic field was set to the maximum of the NO spectrum. The pump frequency was set on the maxima of the nitroxide spectra and a linear chirp pulse (94.9–95.1 GHz) was applied with a duration of 128 ns. The observe frequency was set to 94.8GHz, on the broad so-called 'other

transitions' background (outside the range of the Gd(III) central transition), overlapping with the edge of the nitroxide spectrum (Fig. S4B). The repetition time was set to 200 µs, ensuring saturation of the nitroxide signals and thus eliminating any contribution to the DEER observe signal.

NO–NO DEER**:** The pump frequency was set on the maximum of the nitroxide spectrum and a linear chirp pulse (94.88–94.98 GHz) of a duration of 128 ns was used. The observe frequency was set to 94.85 GHz. The measurement was performed at 35 K with a repletion time of 5 ms.

NMR measurements

All NMR spectra were recorded in 3 mm tubes in NMR buffer at 25 ^{o}C on 600 and 800 MHz Bruker Avance NMR spectrometers equipped with TCI cryoprobes. In all experiments, the concentration of ^{15}N-labelled or ^{15}N,^{13}C-labelled CaM N60D were 0.5 mM and the backbone resonance assignments of CaM N60D were confirmed using HNCA and HN(CO)CA spectra. For the CaM-Ca_3Ln samples (Ln = Y, Tb and Tm), $CaCl_2$ and $LnCl_3$ were added to reach a final concentration of 1.5 mM and 0.5 mM, respectively. For CaM/MARCKS samples, MARCKS peptide was added in 5-fold excess. PCS values were measured in the ^{1}H dimension of the ^{15}N-HSQC spectra.

Data analysis

The time domain DEER data were analyzed using the *DeerAnalysis* 2018 software package.(Jeschke *et al.*, 2006) The Tikhonov regularization was used for the analysis. The background decay was fitted with a dimension of 3 and default values were used for the validation process including noise addition. The Gd(III)-Gd(III) data of the hiolo-CaM in the presence and absence of MARCKS were also analyzed by program GLADD,(Brandon et al., 2012) where the results from each mutant were fitted together constrained to be fitted with the same two Gaussian, albeit with different relative weights in the presence or absence of MARCKS.

Δχ tensor fits

The experimental PCS values measured for CaM N60D-MARCKS peptide complex were used to fit the magnetic susceptibility anisotropy ($\Delta\chi$) tensors to the crystal structure of the CaM-MARCKS

peptide complex (1IWQ) using the program Numbat.(Schmitz *et al.*, 2008) The Ca^{2+} ion coordinates at site II of the crystal structure were used to restrain the metal position during the tensor fits.

Modelling and structure refinement

Distance distributions were predicted from the crystal structures of the Ca^{2+}/CaM/MARCKS complex (PDB ID 1IWQ) and Ca^{2+}/CaM/IQ complex (PDB ID 2BE6, chains A, B and C) using MMM.(Polyhach *et al.*, 2011) The solution structure was obtained using the elastic network model module of the MMM version MMM_2021_2.(Jeschke, 2018) As the restraints are sampled randomly from the Gaussian distribution for each individual we used the ensemble option with 20 runs, where different runs provide an estimate of the uncertainty of the conformation based on the width of the distance distributions.

Acknowledgments

GO thanks the Australian Research Council for a Laureate Fellowship (grant no. FL170100019) and project funding through the Centre of Excellence for Innovations in Peptide and Protein Science, Australian Research Council (grant no. CE200100012). DG acknowledges the support of the Weizmann-UK making connections. DG holds the Erich Klieger Professorial Chair in Chemical Physics.

Author contributions

CJ prepared the samples labelled with nitroxide and DOTA-M and together with AF carried out the spectroscopic measurements and data analysis. SB helped with sample preparation and SN took part in some of the sample preparations and spectroscopic measurements, NM carried out all DEER measurements with the C1 tag their data analysis , EHA prepared all the samples labeled with C1, carried out and analyzed the NMR experiments, GO initiated part of the work and supervised the NMR study, GJ directed the elastic network modeling. DG conceived the study and supervised it. CJ, GO, AF and DG wrote the manuscript, all authors read it.

CJ and AF contributed equally to this work.

Declaration of interests

The authors declare no competing interest.

References

Abdullin, D., Florin, N., Hagelueken, G., and Schiemann, O. (2015). EPR-Based Approach for the Localization of Paramagnetic Metal Ions in Biomolecules. Angew. Chemie. Intl. Ed. *54*, 1827-1831. https://doi.org/10.1002/anie.201410396.

Anthis, N.J., Doucleff, M., and Clore, G.M. (2011). Transient, sparsely populated compact states of apo and calcium-loaded calmodulin probed by paramagnetic relaxation enhancement: interplay of conformational selection and induced fit. J. Am. Chem. Soc. *133*, 18966-18974. 10.1021/ja2082813.

Bahrenberg, T., Rosenski, Y., Carmieli, R., Zibzener, K., Qi, M., Frydman, V., Godt, A., Goldfarb, D., and Feintuch, A. (2017). Improved sensitivity for W-band Gd(III)-Gd(III) and nitroxide-nitroxide DEER measurements with shaped pulses. J. Magn. Reson. *283*, 1-13. 10.1016/j.jmr.2017.08.003.

Bertini, I., Del Bianco, C., Gelis, I., Katsaros, N., Luchinat, C., Parigi, G., Peana, M., Provenzani, A., and Zoroddu, M.A. (2004). Experimentally exploring the conformational space sampled by domain reorientation in calmodulin. Proc. Natl. Acad. Sci. U. S. A. *101*, 6841-6846. 10.1073/pnas.0308641101.

Bertini, I., Gelis, I., Katsaros, N., Luchinat, C., and Provenzani, A. (2003). Tuning the Affinity for Lanthanides of Calcium Binding Proteins. Biochemistry *42*, 8011-8021. 10.1021/bi034494z.

Bertini, I., Gupta, Y.K., Luchinat, C., Parigi, G., Peana, M., Sgheri, L., and Yuan, J. (2007). Paramagnetism-Based NMR Restraints Provide Maximum Allowed Probabilities for the Different Conformations of Partially Independent Protein Domains. J. Am. Chem. Soc. *129*, 12786-12794. 10.1021/ja0726613.

Bertini, I., Kursula, P., Luchinat, C., Parigi, G., Vahokoski, J., Wilmanns, M., and Yuan, J. (2009). Accurate Solution Structures of Proteins from X-ray Data and a Minimal Set of NMR Data: Calmodulin−Peptide Complexes As Examples. J. Am. Chem. Soc. *131*, 5134-5144. 10.1021/ja8080764.

Bertini, I., Luchinat, C., Nagulapalli, M., Parigi, G., and Ravera, E. (2012). Paramagnetic relaxation enhancement for the characterization of the conformational heterogeneity in two-domain proteins. Phys. Chem. Chem. Phys. *14*, 9149-9156. 10.1039/C2CP40139H.

Brandon, S., Beth, A.H., and Hustedt, E.J. (2012). The global analysis of DEER data. J. Magn. Reson. *218*, 93-104. https://doi.org/10.1016/j.jmr.2012.03.006.

Cabrita, L.D., Gilis, D., Robertson, A.L., Dehouck, Y., Rooman, M., and Bottomley, S.P. (2007). Enhancing the stability and solubility of TEV protease using in silico design. Protein Sci. *16*, 2360-2367. 10.1110/ps.072822507.

Chagot, B., and Chazin, W.J. (2011). Solution NMR structure of Apo-calmodulin in complex with the IQ motif of human cardiac sodium channel NaV1.5. J. Mol. Biol. *406*, 106-119. 10.1016/j.jmb.2010.11.046.

Dalaloyan, A., Martorana, A., Barak, Y., Gataulin, D., Reuveny, E., Howe, A., Elbaum, M., Albeck, S., Unger, T., Frydman, V., et al. (2019). Tracking Conformational Changes in Calmodulin in vitro, in Cell Extract, and in Cells by Electron Paramagnetic Resonance Distance Measurements. Chem. Phys. Chem *20*, 1860-1868. https://doi.org/10.1002/cphc.201900341.

Edington, S.C., Gonzalez, A., Middendorf, T.R., Halling, D.B., Aldrich, R.W., and Baiz, C.R. (2018). Coordination to lanthanide ions distorts binding site conformation in calmodulin. Proc. Natl. Acad. Sci. U. S. A. *115*, E3126-E3134. 10.1073/pnas.1722042115.

Fallon, J.L., Halling, D.B., Hamilton, S.L., and Quiocho, F.A. (2005). Structure of calmodulin bound to the hydrophobic IQ domain of the cardiac Ca(v)1.2 calcium channel. Structure *13*, 1881-1886. 10.1016/j.str.2005.09.021.

Giannoulis, A., Ben-Ishay, Y., and Goldfarb, D. (2021). Chapter Eight - Characteristics of Gd(III) spin labels for the study of protein conformations. In Methods Enzymol., J.A. Cotruvo, ed. (Academic Press), pp. 235-290. https://doi.org/10.1016/bs.mie.2021.01.040.

Gifford, J.L., Walsh, M.P., and Vogel, H.J. (2007). Structures and metal-ion-binding properties of the Ca2+-binding helix-loop-helix EF-hand motifs. Biochem. J. *405*, 199-221. 10.1042/bj20070255.

Gigli, L., Andrałojć, W., Dalaloyan, A., Parigi, G., Ravera, E., Goldfarb, D., and Luchinat, C. (2018). Assessing protein conformational landscapes: integration of DEER data in Maximum Occurrence analysis. Phys. Chem. Chem. Phys. *20*, 27429-27438. 10.1039/C8CP06195E.

Glaser, M., Wanaski, S., Buser, C.A., Boguslavsky, V., Rashidzada, W., Morris, A., Rebecchi, M., Scarlata, S.F., Runnels, L.W., Prestwich, G.D., et al. (1996). Myristoylated Alanine-rich C Kinase Substrate (MARCKS) Produces Reversible Inhibition of Phospholipase C by Sequestering Phosphatidylinositol 4,5-Bisphosphate in Lateral Domains. J. Biol. Chem. *271*, 26187-26193. https://doi.org/10.1074/jbc.271.42.26187.

Goldfarb, D., Lipkin, Y., Potapov, A., Gorodetsky, Y., Epel, B., Raitsimring, A.M., Radoul, M., and Kaminker, I. (2008). HYSCORE and DEER with an upgraded 95GHz pulse EPR spectrometer. J. Magn. Reson. *194*, 8-15. 10.1016/j.jmr.2008.05.019.

Her, C., Thompson, A.R., Karim, C.B., and Thomas, D.D. (2018). Structural dynamics of calmodulin-ryanodine receptor interactions: electron paramagnetic resonance using stereospecific spin labels. Sci. Rep. *8*, 10681. 10.1038/s41598-018-29064-8.

Houdusse, A., and Cohen, C. (1995). Target sequence recognition by the calmodulin superfamily: implications from light chain binding to the regulatory domain of scallop myosin. Proc. Natl. Acad. Sci. U. S. A. *92*, 10644-10647. 10.1073/pnas.92.23.10644.

Hovey, L., Fowler, C.A., Mahling, R., Lin, Z., Miller, M.S., Marx, D.C., Yoder, J.B., Kim, E.H., Tefft, K.M., Waite, B.C., et al. (2017). Calcium triggers reversal of calmodulin on nested anti-parallel sites in the IQ motif of the neuronal voltage-dependent sodium channel Na(V)1.2. Biophys. Chem. *224*, 1-19. 10.1016/j.bpc.2017.02.006.

Ikura, M., Clore, G.M., Gronenborn, A.M., Zhu, G., Klee, C.B., and Bax, A. (1992). Solution structure of a calmodulin-target peptide complex by multidimensional NMR. Science *256*, 632-638. 10.1126/science.1585175.

Jeschke, G. (2012a). Characterization of Protein Conformational Changes with Sparse Spin-Label Distance Constraints. J. Chem. Theory Comput. *8*, 3854-3863. 10.1021/ct300113z.

Jeschke, G. (2012b). DEER Distance Measurements on Proteins. Annu. Rev. Phys. Chem. *63*, 419-446. 10.1146/annurev-physchem-032511-143716.

Jeschke, G. (2018). MMM: A toolbox for integrative structure modeling. Protein Sci. *27*, 76-85. https://doi.org/10.1002/pro.3269.

Jeschke, G., Chechik, V., Ionita, P., Godt, A., Zimmermann, H., Banham, J., Timmel, C.R., Hilger, D., and Jung, H. (2006). DeerAnalysis2006—a comprehensive software package for analyzing pulsed ELDOR data. Appl. Magn. Reson. *30*, 473-498. 10.1007/BF03166213.

Kaminker, I., Tkach, I., Manukovsky, N., Huber, T., Yagi, H., Otting, G., Bennati, M., and Goldfarb, D. (2013). W-band orientation selective DEER measurements on a Gd3+/nitroxide mixed-labeled protein dimer with a dual mode cavity. J. Magn. Reson. *227*, 66-71. https://doi.org/10.1016/j.jmr.2012.11.028.

Kataoka, M., Head, J.F., Vorherr, T., Krebs, J., and Carafoli, E. (1991). Small-Angle X-ray Scattering Study of Calmodulin Bound to Two Peptides Corresponding to Parts of the Calmodulin-Binding Domain of the Plasma Membrane Ca^{2+} Pump1 Biochemistry *30*, 6247-6251. 10.1021/bi00239a02.

Kumar, V., Chichili, V.P., Zhong, L., Tang, X., Velazquez-Campoy, A., Sheu, F.S., Seetharaman, J., Gerges, N.Z., and Sivaraman, J. (2013a). Structural basis for the interaction of unstructured neuron specific substrates neuromodulin and neurogranin with Calmodulin. Sci Rep *3*, 1392. 10.1038/srep01392.

Kumar, V., Chichili, V.P.R., Zhong, L., Tang, X., Velazquez-Campoy, A., Sheu, F.-S., Seetharaman, J., Gerges, N.Z., and Sivaraman, J. (2013b). Structural Basis for the Interaction of Unstructured Neuron Specific Substrates Neuromodulin and Neurogranin with Calmodulin. Sci. Rep. *3*, 1392. 10.1038/srep01392.

Lafitte, D., Heck, A.J., Hill, T.J., Jumel, K., Harding, S.E., and Derrick, P.J. (1999a). Evidence of noncovalent dimerization of calmodulin. Eur. J. Biochem. *261*, 337-344. 10.1046/j.1432-1327.1999.00284.x.

Lafitte, D., Heck, A.J.R., Hill, T.J., Jumel, K., Harding, S.E., and Derrick, P.J. (1999b). Evidence of noncovalent dimerization of calmodulin. European Journal of Biochemistry *261*, 337-344. https://doi.org/10.1046/j.1432-1327.1999.00284.x.

Lueders, P., Jeschke, G., and Yulikov, M. (2011). Double Electron−Electron Resonance Measured Between Gd3+ Ions and Nitroxide Radicals. J. Phys. Chem. Lett. *2*, 604-609. 10.1021/jz200073h.

Marko, A., Denysenkov, V., Margraf, D., Cekan, P., Schiemann, O., Sigurdsson, S.T., and Prisner, T.F. (2011). Conformational Flexibility of DNA. J. Am. Chem. Soc. *133*, 13375-13379. 10.1021/ja201244u.

Martorana, A., Bellapadrona, G., Feintuch, A., Di Gregorio, E., Aime, S., and Goldfarb, D. (2014). Probing Protein Conformation in Cells by EPR Distance Measurements using Gd3+ Spin Labeling. J. Am. Chem. Soc. *136*, 13458-13465. 10.1021/ja5079392.

Matsubara, M., Yamauchi, E., Hayashi, N., and Taniguchi, H. (1998). MARCKS, a major protein kinase C substrate, assumes non-helical conformations both in solution and in complex with Ca2+-calmodulin. FEBS Lett. *421*, 203-207. 10.1016/s0014-5793(97)01557-3.

Maximciuc, A.A., Putkey, J.A., Shamoo, Y., and Mackenzie, K.R. (2006). Complex of calmodulin with a ryanodine receptor target reveals a novel, flexible binding mode. Structure *14*, 1547-1556. 10.1016/j.str.2006.08.011.

Meador, W., Means, A., and Quiocho, F. (1992). Target enzyme recognition by calmodulin: 2.4 A structure of a calmodulin-peptide complex. Science *257*, 1251-1255. 10.1126/science.1519061.

Neylon, C., Brown, S.E., Kralicek, A.V., Miles, C.S., Love, C.A., and Dixon, N.E. (2000). Interaction of the Escherichia coli replication terminator protein (Tus) with DNA: a model derived from DNA-

binding studies of mutant proteins by surface plasmon resonance. Biochemistry *39*, 11989-11999. 10.1021/bi001174w.

Ogawa, Y., and Tanokura, M. (1984). Calcium binding to calmodulin: effects of ionic strength, Mg2+, pH and temperature. J. Biochem. *95*, 19-28. 10.1093/oxfordjournals.jbchem.a134584.

Osawa, M., Tokumitsu, H., Swindells, M.B., Kurihara, H., Orita, M., Shibanuma, T., Furuya, T., and Ikura, M. (1999). A novel target recognition revealed by calmodulin in complex with Ca2+-calmodulin-dependent kinase kinase. Nat. Struct. Biol. *6*, 819-824. 10.1038/12271.

Otting, G. (2008). Prospects for lanthanides in structural biology by NMR. J. Biomol. NMR *42*, 1-9. 10.1007/s10858-008-9256-0.

Pannier, M., Veit, S., Godt, A., Jeschke, G., and Spiess, H.W. (2000). Dead-time free measurement of dipole-dipole interactions between electron spins. J. Magn. Reson. *142*, 331-340. 10.1006/jmre.1999.1944.

Polyhach, Y., Bordignon, E., and Jeschke, G. (2011). Rotamer libraries of spin labelled cysteines for protein studies. Phys. Chem. Chem. Phys *13*, 2356-2366. 10.1039/C0CP01865A.

Porumb, T., Crivici, A., Blackshear, P.J., and Ikura, M. (1997a). Calcium binding and conformational properties of calmodulin complexed with peptides derived from myristoylated alanine-rich C kinase substrate (MARCKS) and MARCKS-related protein (MRP). Eur. Biophys. J *25*, 239-247. 10.1007/s002490050036.

Porumb, T., Crivici, A., Blackshear, P.J., and Ikura, M. (1997b). Calcium binding and conformational properties of calmodulin complexed with peptides derived from myristoylated alanine-rich C kinase substrate (MARCKS) and MARCKS-related protein (MRP). Eur. Biophys. J *25*, 239-247. 10.1007/s002490050036.

Potter, J.D., Strang-Brown, P., Walker, P.L., and Iida, S. (1983). Ca2+ binding to calmodulin. Methods Enzymol. *102*, 135-143. 10.1016/s0076-6879(83)02014-5.

Puljung, M.C., DeBerg, H.A., Zagotta, W.N., and Stoll, S. (2014). Double electron–electron resonance reveals cAMP-induced conformational change in HCN channels. Proc. Natl. Acad. Sci. U. S. A. *111*, 9816. 10.1073/pnas.1405371111.

Qin, Z., Wertz, S.L., Jacob, J., Savino, Y., and Cafiso, D.S. (1996). Defining protein-protein interactions using site-directed spin-labeling: the binding of protein kinase C substrates to calmodulin. Biochemistry *35*, 13272-13276. 10.1021/bi961747y.

Russo, L., Maestre-Martinez, M., Wolff, S., Becker, S., and Griesinger, C. (2013). Interdomain Dynamics Explored by Paramagnetic NMR. J. Am. Chem. Soc. *135*, 17111-17120. 10.1021/ja408143f.

Schmitz, C., Stanton-Cook, M.J., Su, X.-C., Otting, G., and Huber, T. (2008). Numbat: an interactive software tool for fitting Δχ-tensors to molecular coordinates using pseudocontact shifts. J. Biomol. NMR *41*, 179. 10.1007/s10858-008-9249-z.

Schumacher, M.A., Rivard, A.F., Bächinger, H.P., and Adelman, J.P. (2001). Structure of the gating domain of a Ca2+-activated K+ channel complexed with Ca2+/calmodulin. Nature *410*, 1120-1124. 10.1038/35074145.

Smith, P.K., Krohn, R.I., Hermanson, G.T., Mallia, A.K., Gartner, F.H., Provenzano, M.D., Fujimoto, E.K., Goeke, N.M., Olson, B.J., and Klenk, D.C. (1985). Measurement of protein using bicinchoninic acid. Anal. Biochem. *150*, 76-85. 10.1016/0003-2697(85)90442-7.

Thomas, C.M., and Timson, D.J. (2018). Calmodulins from Schistosoma mansoni: Biochemical analysis and interaction with IQ-motifs from voltage-gated calcium channels. Cell Calcium *74*, 1-13. 10.1016/j.ceca.2018.05.006.

Vetter, S.W., and Leclerc, E. (2003). Novel aspects of calmodulin target recognition and activation. Eur. J. Biochem. *270*, 404-414. 10.1046/j.1432-1033.2003.03414.x.

Wu, P.S., Ozawa, K., Lim, S.P., Vasudevan, S.G., Dixon, N.E., and Otting, G. (2007). Cell-free transcription/translation from PCR-amplified DNA for high-throughput NMR studies. Angew. Chem., Int. Ed. Engl. *46*, 3356-3358. 10.1002/anie.200605237.

Yamauchi, E., Nakatsu, T., Matsubara, M., Kato, H., and Taniguchi, H. (2003). Crystal structure of a MARCKS peptide containing the calmodulin-binding domain in complex with Ca2+-calmodulin. Nat. Struct. Biol. *10*, 226-231. 10.1038/nsb900.

Yamniuk, A.P., and Vogel, H.J. (2004). Calmodulin's flexibility allows for promiscuity in its interactions with target proteins and peptides. Mol. Biotechnol. *27*, 33-57. 10.1385/MB:27:1:33.

Yap, K.L., Kim, J., Truong, K., Sherman, M., Yuan, T., and Ikura, M. (2000). Calmodulin target database. J. Struct. Funct. Genomics *1*, 8-14. 10.1023/a:1011320027914.

Ye, L., Van Eps, N., Li, X., Ernst, O.P., and Prosser, R.S. (2017). Utilizing tagged paramagnetic shift reagents to monitor protein dynamics by NMR. Biochim. Biophys. Acta, Proteins Proteomics *1865*, 1555-1563. 10.1016/j.bbapap.2017.09.011.

Figure legends

Crystal structure of *holo*-CaM bound peptides

Figure 1. Crystal structures of (A) *holo*-CaM/IQ (PDB 2BE6, chain A)(Fallon *et al.*, 2005) and (B) *holo*-CaM/MARCKS (PDB 1IWQ).(Yamauchi *et al.*, 2003) The C-domain is colored deep teal, the N-domain light orange and bound peptide pink. The Gd(III) ion replacing one of the Ca^{2+} ions in the N60D mutant is indicated in red and the Ca^{2+} ions are green. CaM and peptide residues labelled with tags are identified by red and purple balls, respectively. Lines connecting the labelling sites indicate pairs subjected to DEER measurements (C) Superimposition of the structures shown in (A) and (B). The positions of some of the labelling sites are shown in red and blue for the complex with the MARCKS and IQ peptide, respectively. The IQ peptide is shown in magenta and the MARCKS peptide in cyan. The structure 2BE6 is colored yellow and 1IWQ green.

Structures of the spin labels

Figure 2. Spin labels used in this study.

DEER data of free and peptide bound CaM double mutants

Figure 3. DEER data of Ca^{2+}-CaM labelled in different ways, free and with MARCKS or IQ peptides. (A) Gd(III)–Gd(III) DEER of the mutant T34C/T117C-Gd-DOTA-M. (B) Gd(III)–NO DEER of the mutant T34C-MA-proxyl/N60D-Gd(III). (C) Gd(III)–NO DEER of the mutant T117C-MA-

proxyl/N60D-Gd(III). The panels on the left show the DEER data after the background removal along with the fitted trace. Traces that had low modulation depth were expanded by a factor as noted in the figure. The panels in the middle column show the corresponding distance distributions along with the distance distribution predicted from the respective crystal structures (blue, using chain A for the IQ data). The colour bar underneath the distance distributions shows the reliability regions as defined in DeerAnalysis, determined by the DEER evolution time (green: the shape of the distance distribution is reliable; yellow: the mean distance and distribution width are reliable; orange: the mean distance is reliable; red: unreliable long-range distances). The solid lines represent the distributions with the smallest r.m.s.d. to the experimental data and the striped regions indicate the range of alternative distributions ($\pm$2 times the standard deviation) obtained by varying the parameters of the background correction and noise as calculated by the validation tool in the DeerAnalysis software package with the default values.(Jeschke *et al.*, 2006) The primary DEER data are shown in Fig. S6. The right column presents cartoons of CaM with the labelling sites.

DEER data of MARCKS peptide bound to *apo*- and *holo*-CaM single mutants

Figure 4. Gd(III)–NO DEER data of *holo*-CaM (black) and *apo*-CaM (red) in the presence of MARCKS peptide. The left column shows the DEER data after background subtraction with the corresponding fits. The middle column shows the associated distance distributions. Uncertainty ranges are indicated as in Figure 3. The blue line represents the predicted distance distribution from the crystal structure 2BE6, chain A, calculated using the MMM software. The last column shows cartoons of the CaM/MARCKS complex indicating the labelling scheme. The primary DEER data are given in Fig. S11.

DEER data of IQ peptide bound to *apo*- and *holo*-CaM single mutants

Figure 5. Gd(III)–NO DEER data of *holo*-CaM (black) and *apo*-CaM (red) in the presence of (A) C-IQ or (B) N-IQ peptide. The left column shows the DEER data after background subtraction with the corresponding fits. The middle column shows the associated distance distributions. Uncertainty ranges are indicated as in Figure 3. The blue line represents the predicted distance distribution from the crystal structure 2BE6 (chain A).

^{15}N-HSQC spectra of 0.5 mM solutions of CaM N60D with MARCKS peptide

Figure 6. Superimposition of ^{15}N-HSQC spectra of 0.5 mM solutions of CaM N60D with MARCKS peptide. The concentrations of CaM N60D, MARCKS peptide, $CaCl_2$ and $LnCl_3$ were 0.5 mM, 2.5 mM, 1.5 mM and 0.5 mM, respectively. Spectra with diamagnetic Y(III) are in black, and with paramagnetic Tb(III) and Tm(III) in blue and red, respectively. Selected sets of cross-peaks in the diamagnetic and paramagnetic samples are connected by lines and labelled with their resonance assignment. (a) Uniformly ^{15}N-labelled CaM N60D. (b) Selectively ^{15}N-alanine, ^{15}N-methionine and ^{15}N-valine-labelled CaM N60D.

PCSs for CaM N60D in complex with MARCKS peptide

Figure 7. Correlations between back-calculated and experimental PCSs for CaM N60D in complex with MARCKS peptide. (a) Correlation for the amide protons of the N-domain. Blue and red points mark the PCSs obtained with Tb(III) and Tm(III), respectively. (b) Same as (a) but for the C-domain.

Correlation between experimental PCSs for free and MARCKS bound *holo*-CaM

Figure 8. Correlations between experimental PCSs measured for free *holo*-CaM N60D (Bertini *et al.*, 2004) and CaM N60D in complex with MARCKS peptide. (a) Correlation for the amide protons of the N-domain. Blue and red points mark the PCSs obtained with Tb(III) and Tm(III), respectively. (b) Same as (a) but for the C-domain.

Modeled structure of the solution structure from elastic network model

Figure 9. Two views of the ensemble of 20 structures obtained from fitting the distance distributions using the elastic network model, using the experimental results obtained with all constructs of *holo*-CaM in complex with IQ peptide as restraints (twelve in total). The calculations were performed by setting the restraints obtained with *holo*-CaM T117C-Ma-proxy/N60D-Gd(III) either to average (av), short or long distances. The magenta ribbon corresponds to the crystal structure 2BE6, chain A. The Ca^{2+} ions are shown as green balls. The position of the Gd(III) ion in the N60D mutant is identified by an arrow. The IQ peptide is shown in pink, the N-domain in gold, and the C-domain in deep teal.

Comparison of experimental and modeled distance distributions

Figure 10. Comparison of the distance distributions in the structures fitted with the long distance restraint option (blue), distance distributions modelled on the X-ray structure (black) and the experimental results (red) for all constructs of *holo*-CaM. The T117C-MA-proxyl/N60D-Gd(III) construct shows a second distribution with a short distance, which is not accounted for by either the model or crystal structure.